Adsorption at nanostructured surfaces

Axel Groß
Physik-Department T30
Technische Universität München
85747 Garching/Germany

Phone: +49 89 289 12355
Fax: +49 89 289 12296
email: agross@ph.tum.de

Contents

I. INTRODUCTION

There is a strong current interest in the adsorption of atoms and molecules at nanostructured surfaces. This interest is fueled by the general attention that nanoscience and nanotechnology has received in recent years. Systems with reduced dimensions can exhibit surprising chemical, mechanical, vibrational, electronic, magnetic or optical properties that are distinctly different from those of extended systems. Consequently, also the adsorption properties of molecules can be significantly modified by nanostructuring a substrate.

However, as far as the interaction with molecules is concerned, surfaces with structures at the nanometer scale have already played a significant technological role for many years, long before the advent of nanotechnology, in particular in the field of heterogeneous catalysis. One of the most prominent example is the car exhaust catalyst, where small metal particles on an oxide support are the catalytically active species [1–4]. In fact, the activity of many real catalysts is often assumed to be dominated by so-called *active sites*, i.e., sites with a specific geometric configuration on the nanometer scale that modifies their electronic and chemical properties. However, experimentally it is almost impossible to deduce the exact nature of these active sites.

Ideally, one would like to have a systematic microscopic understanding of the relationship between the geometric and electronic structure of a substrate and its adsorption properties and reactivity. This would allow the systematic tailoring of its activity, but requires a detailed atomistic knowledge about the investigated nanostructures. The development of the scanning tunneling microscope (STM) [5] was an experimental milestone allowing the imaging of structures and processes on surfaces with atomic resolution. Still, one has to keep in mind that the STM does not directly yield the atomic structure but rather images the electronic density of states [6]. Therefore sometimes it is not easy to identify the atomic structure underlying a particular STM image. Furthermore, nanostructured surfaces with a strong corrugation are hard to image because the finite size of the STM tip leads to a limited lateral resolution [7]. Therefore the size and shape of, e.g., supported clusters are often not really known. It is true that the deposition of size-selected clusters together with soft-landing techniques allows the preparation of a monodispers distribution of supported clusters [8]. Yet, the exact structure of the soft-landed clusters is also known either.

Theoretical studies, on the other hand, have the advantage that they deal with well-defined systems. This means that the microscopic structure of the studied systems is of course predetermined by the theorist performing the calculations. Because of the tremendous progress in the computer power and the development of efficient electronic structure algorithms, a very fruitful and close collaboration between theory and experiment for the investigation of interaction of atoms and molecules with surfaces and nanostructures has become possible [9, 10]. In the early days of theoretical surface science, quantum chemistry methods [11] based on representations of the electronic many-body wave function had prevailed. Unfortunately, wave function based methods are limited to rather small systems because of their unfavorable scaling with the size of the treated systems. Nowadays, the *ab initio* treatment of surfaces and nanostructures is dominated by total energy calculations based on density functional theory (DFT) [12–15] which combine numerical efficiency with a satisfactory reliability and accuracy.

A broad variety of surface properties can now be described from first principles, i.e. without invoking any empirical parameters [16]. First of all, *ab initio* total-

energy calculations allow the determination of the equilibrium structure of a specific system. However, these calculations offer even more. They also yield the electronic structure underlying a particular optimum geometry. The analysis of the electron structure and its interpretation within a conceptual framework can lead to a general understanding of the principles underlying adsorbates structures, chemical trends and the relation between reactivity and structure. In order to make such an understanding possible, it is very important to establish reactivity concepts. These allow to categorize the immense variety of possible structures and reactions.

In this review, I will mainly focus on two types of nanostructured surfaces: stepped surfaces and supported clusters. It is true, however, that the nanostructures that can be addressed presently by electronic structure calculations are still very limited in size. For example, the separation of the steps treated in theoretical studies is often smaller than the corresponding separation of steps studied in experiments [17], and typically supported clusters with less than 10 atoms are treated in the calculations while the clusters studied in experiments often contain more than one thousand atoms [18]. Hence, there is still a gap between the nanostructure sizes dealt with in theory and in experiment.

Nevertheless, it is still possible to extract qualitative trends from theoretical studies, for example as far as the role of low-coordinated sites at the nanostructures is concerned. Furthermore, modern experimental cluster sources together with soft-landing techniques allow the deposition of clusters with basically any desired number of atoms well below one hundred. In addition, the improvement in computer power and the efficiency of the computer codes will make it possible to address larger and larger systems. Thus we will certainly see an ongoing closing of the gap between experiment and theory in the future. It should also be emphasized that the application of large scale electronic structure calculations to surfaces and nanostructures is a relatively young field. While the first detailed *ab initio* calculations of the interaction of molecules with low-index surfaces started in the early 1990s [19–22], the treatment of nanostructured surfaces became only possible in the new millenium except for a few studies that were carried out on supercomputers in the 1990s [8, 23].

The topic of this review is the adsorption of atoms and molecules on nanostructured surfaces. However, adsorption studies are often performed in order to understand the reactivity of a particular nanostructure. Hence studies of adsorption and reactions on nanostructures are often closely related. Therefore I will also briefly discuss the chemical reactions which are promoted by specific nanostructures. Furthermore, I will not only address adsorbates on nanostructured surfaces, but also nanostructuring by adsorbates, mainly by organic molecules, which might be useful for sensing, catalysis, or molecular electronics.

Instead of giving a comprehensive overview over many systems, I will focus on particular well-studied systems which allow to manifest qualitative trends for the interaction of atoms and molecules with nanostructured surfaces. In particular, as far as the adsorption on supported clusters is concerned, I will mainly discuss the Au/TiO_2 system [18, 24, 25] which has become *the* model system for the understanding of the chemical reactivity of supported nanoparticles. This system is of particular interest because bulk Au is chemically inert in contrast to the Au nanoparticles, so that its study allows the identification of the geometric and electronic factors underlying the enhanced reactivity of nanoparticles.

This chapter is structure as follows. In the next section, a brief introduction into the theoretical concepts needed for the first-principles description of adsorption on nanostructured surfaces will be given. The third section is devoted to the adsorption on stepped surfaces, while the fourth section covers the adsorption on supported nanoparticles. Then there will be a brief introduction into the nanostructuring of surfaces by organic templates. Finally some conclusions and an outlook will be given where possible directions of further research will be sketched.

II. THEORETICAL CONCEPTS

In the realm of chemistry and solid-state physics, only the kinetic energy and the electrostatic interaction enter the basic expresssion for the total energy of a physical system. Because of their light mass, the electrons have to be treated quantum mechanically. Thus a theoretical analysis "just" requires the solution of the appropriate quantum many-body Schrödinger equation. Unfortunately, the exact analytical solution of the Schrödinger equation for any realistic many-body system is not possible. Consequently, only approximate numerical solutions can be obtained, but they should be as reliable and as accurate as possible, and at the same time they should not be computationally too demanding so that the calculations can be carried out within a reasonable time.

The first calculations of surface structures were based on quantum chemistry methods [11, 26, 27] in which the Schrödinger equation is solved using necessarily finite basis sets for the wave functions. The theoretical tools used by quantum chemists are designed to describe finite systems such as molecules. In the quantum chemistry approach, surfaces are regarded as big molecules and modeled by a finite cluster. This ansatz is guided by the idea that bonding on surfaces is a local process. These methods significantly contributed to our understanding of processes at surfaces (see, e.g., [28, 29]). However, these calculations become prohibitively expensive for larger systems because of their unfavorable scaling with the system size. Nowadays, predominantly electronic structure calculations using density functional theory (DFT) [12, 13] are performed. They offer a good compromise between computational efficiency and suffi-

cient accuracy for many systems. Still, there are important exceptions where present-day DFT methods are not accurate enough [30, 31].

Here I will only give a brief sketch of the fundamentals of DFT which are important for a general understanding. Historically, the first attempts to relate the electronic density and the total energy were made within the framework of the Thomas-Fermi theory [32] which is only valid in the limit of slowly varying electron density. Hohenberg and Kohn extended this relation also to inhomogeneous situations [12]. The Hohenberg-Kohn theorem states that the exact ground-state density and energy can be determined by the minimization of the energy functional $E[n]$,

$$E_{\rm tot} = \min_{n(\vec{r})} E[n] = \min_{n(\vec{r})} (T[n] + V_{\rm ext}[n] + V_{\rm H}[n] + E_{\rm xc}[n]) \ , \tag{1}$$

which means that there is a one-to-one correspondence between the electron ground-state density $n(\vec{r})$ and the total energy. In eq. (1), $V_{\rm ext}[n]$ and $V_H[n]$ are the functionals of the external potential and of the classical electrostatic interaction energy, respectively, while $T[n]$ is the kinetic energy functional for non-interacting electrons. These three terms do not contain any quantum mechanical many-body effects which are all lumped together in the so-called *exchange-correlation* functional $E^{\rm xc}[n]$ that is, unfortunately, not known in general.

It had turned out that the Hohenberg-Kohn theorem is not useful for a direct implementation of the DFT, mainly because the kinetic energy functional $T[n]$ is not precisely known for inhomogeneous situations. One rather replaces the many-body Schrödinger equation by a set of coupled effective one-particle equations, the so-called Kohn-Sham equations [13]

$$\left\{ -\frac{\hbar^2}{2m}\nabla^2 + v_{ext}(\vec{r}) + v_{\rm H}(\vec{r}) \ + \ v_{\rm xc}(\vec{r}) \right\} \psi_i(\vec{r}) = \varepsilon_i \, \psi_i(\vec{r}) \ , \tag{2}$$

where $v_{\rm ext}$ is the external potential and the *Hartree potential* $v_{\rm H}$ is given by

$$v_{\rm H}(\vec{r}) = \int d^3\vec{r}' n(\vec{r}') \frac{e^2}{|\vec{r} - \vec{r}'|} \ . \tag{3}$$

The exchange-correlation potential $v_{\rm xc}(\vec{r})$ is the functional derivative of the exchange-correlation functional $E_{\rm xc}[n]$

$$v_{\rm xc}(\vec{r}) = \frac{\delta E_{\rm xc}[n]}{\delta n} \ . \tag{4}$$

The electron density $n(\mathbf{r})$ which minimizes the total energy is then given by the sum over single-particle Kohn-Sham states

$$n(\vec{r}) = \sum_{i=1}^{N} \ |\psi_i(\vec{r})|^2 \ . \tag{5}$$

The ground state energy can now be expressed as

$$E = \sum_{i=1}^{N} \ \varepsilon_i + E_{\rm xc}[n] - \int v_{\rm xc}(\vec{r}) n(\vec{r}) \ d^3\vec{r} - V_{\rm H} \ . \tag{6}$$

The first term in the total-energy expression (6) is also called the band structure term $E_{\rm bs}$ since it corresponds to the sum over the single-particle energies.

There is one complication as far as the solution of the Kohn-Sham equations is concerned. The electron density $n(\vec{r})$ which is derived from the Kohn-Sham states actually enters the effective one-particle Hamiltonians, i.e. the exact Hamiltonians are not known *a priori*. In such a situation, the solutions can be obtained within an iterative self-consistency scheme. Initially the electron density has to be guessed, for example as a superposition of atomic densities. The Kohn-Sham equations are then solved and the resulting density is compared to the initial guess. If the difference is larger than some pre-specified value, the new density enters the Kohn-Sham equations (often using some mixing scheme), and the cycle is repeated so often until the iterations no longer modify the solutions, i.e. until self-consistency is reached.

In principle, DFT is exact, but as already mentioned, the correct form of the non-local exchange-correlation functional is not known. This also applies to the exchange-correlation potential v_{xc}. Hence approximative expressions are needed. In the local density approximation (LDA), at any position $\vec{r}$ the exchange-correlation potential of the homogeneous electron gas with the corresponding electron density is used. This means that non-local effects in the exchange and correlation are entirely neglected. Although this is a rather crude approximation, the LDA has been surprisingly successful for many properties of bulk materials. However, for chemical reactions at surface LDA is not sufficiently accurate [20]. Satisfactory accuracy is obtained within the so-called generalized gradient approximation (GGA) [33] which takes the gradient of the density also into account in the exchange-correlation functional, but in such a way that important electronic sum rules are obeyed. GGA represents the state of the art for large scale DFT calculations of surfaces and nanostructures.

There are quite a number of different GGA functionals available. While quantum chemists using DFT prefer exchange-correlation functionals that are fitted to a number of reference reactions in the gas phase [34, 35], physicists rather rely on functionals that are derived without any adjustment of parameters [33, 36]. It should be mentioned that GGA calculations do not achieve *chemical accuracy* (error below ∼0.1 eV) for all systems and that there can be quite significant quantitative discrepancies between the results of DFT calculations using different GGA functionals.

For example, there are two versions of the popular GGA functional developed by Perdew, Burke and Ernzerhof, called the PBE functional [36] and the revised PBE, RPBE [30]. Both versions differ only by one interpola-

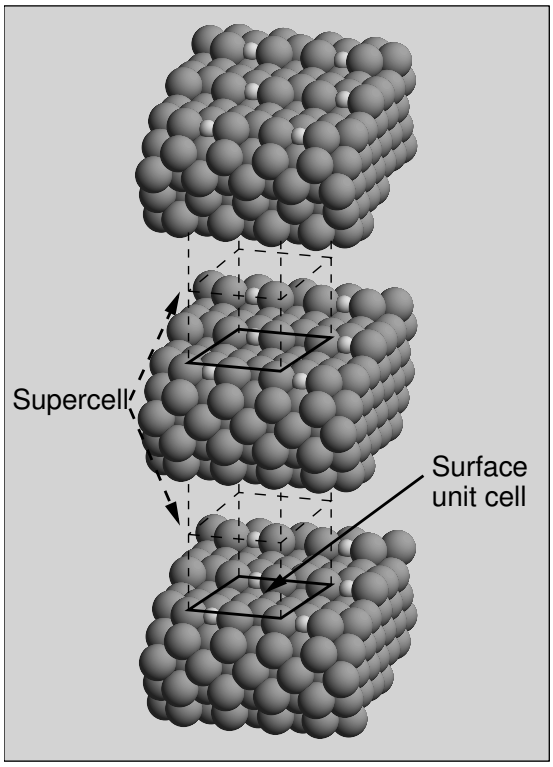

FIG. 1: Illustration of the supercell approach. A substrate of a fcc crystal with a (410) surface termiantion and an adsorbed periodic atomic layer in a (2×12) geometry is represented by an infinite array of slabs. The supercell and the surface unit cell are indicated in the figure.

tion function which is not specified in the construction scheme for the functional. Hence there is no way to tell *a priori* which is the more correct functional. Still, for certain systems there are differences of up to 0.5 eV between the results using these two functionals, in particular as far as the adsorption energies of O_2, NO or CO on metal surfaces are concerned [30]. Fortunately, often this only leads to quantitative but not qualitative differences or errors. Nevertheless, there are also systems where all present GGA functionals yield wrong qualitative results, for example for the adsorption site of CO on Pt(111) [31]. In most cases, DFT-GGA calculations are actually reliable, but one still should always be cautious and compare the DFT results with available experimental data.

Hence, the search for more accurate exchange-correlation functionals is an active research field [37, 38]. However, the problem in the development of more accurate exchange-correlation functionals is that they still represent in principle an uncontrolled approximation, i.e., there is no systematic way of improving the functionals since there is no expansion in some small, controllable parameter.

As far as the practical implementation of DFT algorithms is concerned, it is numerically very efficient to use a plane-wave expansion of the Kohn-Sham single-particle states. However, such an approach usually require a three-dimensional periodicity of the considered system. In the so-called supercell approach, surfaces are modeled by periodically repeated slabs with a sufficient vacuum layer between them in order to avoid any interaction between the slabs. A typical supercell describing the adsorption of atoms at the step sites of a nanostructured fcc(410) surface in a (2×1) geometry is shown in Fig. 1. The slabs have to be thick enough to reproduce the correct electronic structure of the substrate. One advantage of the slab approach is that the substrates are infinitely extended in lateral directions which yields a correct description of the delocalized nature of the electronic states of metals, a feature that is not present when the substrates are modeled by finite clusters [29].

On the basis of total-energy calculations, adsorption energies and reaction barrier heights are determined as the differences of the total energies of the appropriate systems. For example, the adsorption energy $E_{\rm ads}$ of a molecule can be determined via

$$E_{\rm ads} \;=\; (E_{\rm slab} \,+\, E_{\rm mol}) \;-\, E_{\rm slab+mol}\;, \qquad (7)$$

where $E_{\rm slab}$, $E_{\rm mol}$ and $E_{\rm slab+mol}$ are the total energies per unit cell of the isolated slab, the isolated molecule and the interacting system, respectively. Using this definition, the exothermic adsorption of molecules is represented by positive energies, as will be done throughout this chapter. However, often the sign convention is also chosen to be the other way around.

In any implementation of DFT, the computational effort is directly linked to the number of electrons that have to be taken into account. Now most chemical and materials properties are governed almost entirely by the valence electrons while the influence of the core electrons on these properties is negligible. This fact is used in the pseudopotential concept [39] in which the influence of the core electrons on the other electrons is represented by an effective potential, the pseudopotential. Since this significantly reduces the number of electrons that have to be taken into account, the use of pseudopotentials leads to an enormous saving of computer time.

A further significant improvement has been the formulation of the projected augmented-wave (PAW) method [40] and the development of *ultra-soft* pseudopotentials [41]. Both methods are indeed closely related [42]. They introduce augmentation charges in the core region in order to create smooth potentials which results in a dramatic reduction in the necessary size of the basis set in plane-wave calculations.

Almost all modern DFT studies presented in this chapter employ the pseudopotential concept, and many large-scale computations would be impossible without the use of pseudopotentials. Using the supercell technique in combination with the pseudopotential or PAW concept, modern efficient DFT algorithms [43–45] can treat up to several hundreds or even thousands of atoms per supercell (see, e.g., [46]).

DFT calculations not only yield total energies but also information about the electronic structure. First of all,

plots of the total charge density are useful in order to get an idea of the nature of the chemical binding. However, even more instructive is the analysis of charge density difference plots, for example of the adsorption induced charge density difference

$$n_{\rm diff}(\vec{r}) \;=\; n_{\rm total}(\vec{r}) \,-\, n_{\rm adsorbate}(\vec{r}) \,-\, n_{\rm substrate}(\vec{r}) \;. \quad (8)$$

These charge density difference plots illustrate the charge redistribution and the rehybridization due to the interaction of the reactants. Hence they allow the determination of charge transfer processes, and even the nature and symmetry of the involved orbitals can be deduced from the spatial patterns.

However, not only the electronic structure in real space, but also in momentum and energy space yields valuable information. In particular the determination of changes in the local density of states (LDOS) which is defined by

$$n(\vec{r},\varepsilon) \;=\; \sum_i \; |\phi_i(\vec{r})|^2 \; \delta(\varepsilon - \varepsilon_i) \;. \quad (9)$$

adds additional information about the electronic orbitals and bands that are involved in the adsorption process.

Still, for a deeper understanding of, e.g., chemical trends qualitative concepts are needed that allow an fundamental analysis and interpretation of the electronic structure. A rather simple but still very useful reactivity concept was derived by Hammer and Nørskov [47, 48], the so-called *d*-band model. This scheme is closely related to the frontier orbital concept developed for gas-phase reactions [49, 50]. In the *d*-band model, the whole *d*-band is replaced by an effective level located at the center of the *d*-band ε_d. This level plays the role of the substrate frontier orbitals, i.e. of the highest occupied molecular orbital (HOMO) and the lowest unoccupied molecular orbital (LUMO).

The principles underlying the *d*-band model are illustrated in Fig. 2. Let us first consider the interaction of an atomic level with a transition metal surface. This interaction is formally split into a contribution arising from the *s* and *p* states of the metal and a second contribution coming from the *d*-band. The *s* and *p* states lead to a broadening and a shift of the atomic level to lower energies. This broadening and shift is called *renormalization* of the energy level and can be modelled by the interaction with a jellium surface.

This renormalized level then splits due to the strong hybridization with the metal *d*-states in a bonding and an anti-bonding contribution. Both the strength of the interaction as well as the position of the center of the *d*-band ε_d determine whether the interaction is attractive or repulsive. The stronger the interaction, the more the two levels are split. A very strong interaction shifts the bonding orbital to lower energies. Furthermore, it pushes the anti-bonding contribution above the Fermi energy. Both effects lead to an effective attractive interaction.

As Fig. 2 illustrates, the position of the center of the *d*-band ε_d determines the occupation of the bonding and

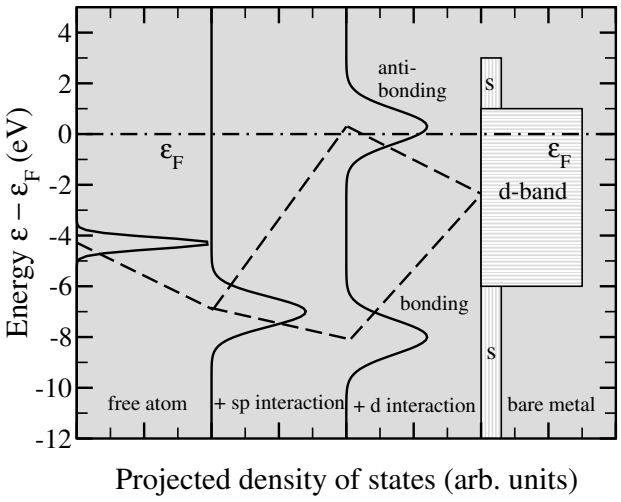

FIG. 2: Schematic drawing of the interaction of an atomic level with a transition metal surface according to the *d*-band model [47].

the anti-bonding contribution. The higher the *d*-band center, the smaller the occupation of the anti-bonding level and the more attractive the interaction. Therefore, transition metals are rather reactive since the Fermi energy is rather close to the *d*-band center because of the only partially filled *d*-band. For a noble metal, on the other hand, the *d*-band center is so low that both the bonding *and* the anti-bonding state of adsorbate-substrate interaction are occupied making this interaction repulsive. This is the reason why noble metals are noble, i.e., less reactive than transition metals [48].

The *d*-band model is particularly useful for comparing the reactivity of relatively similar systems which only differ in the position of the *d*-band center. Then there is a linear relationship between the *d*-band center shift and the change in the chemisorption strength ΔE_d [51, 52],

$$\delta E_d = -\frac{V^2}{|\epsilon_d - \epsilon_a|^2} \; \delta\varepsilon_d \;, \quad (10)$$

which means that there is a stronger interaction or larger energy gain upon an upshift of the *d*-band.

This concept provides an intuitive picture for the enhanced reactivity of nanostructured surfaces which is illustrated in Fig. 3. Consider a typical transition metal with a more than half-filled *d*-band (Fig. 3a). At a step atom or at some other low-coordinated site, the local *d*-band density of states will be changed. In a simple tight-binding picture, the width of a band is directly related to the coordination and the overlap of the orbitals. At a low-coordinated site, the *d*-band will therefore become narrower (see Fig. 3b, the same is also true for pseudomorphic overlayers under tensile strain which reduces the overlap between the electronic orbitals [53–55]). Now if the *d*-band is more than half-filled but not completely filled and the *d*-band center is kept fixed, the number of *d*-states below the Fermi energy will increase. This would

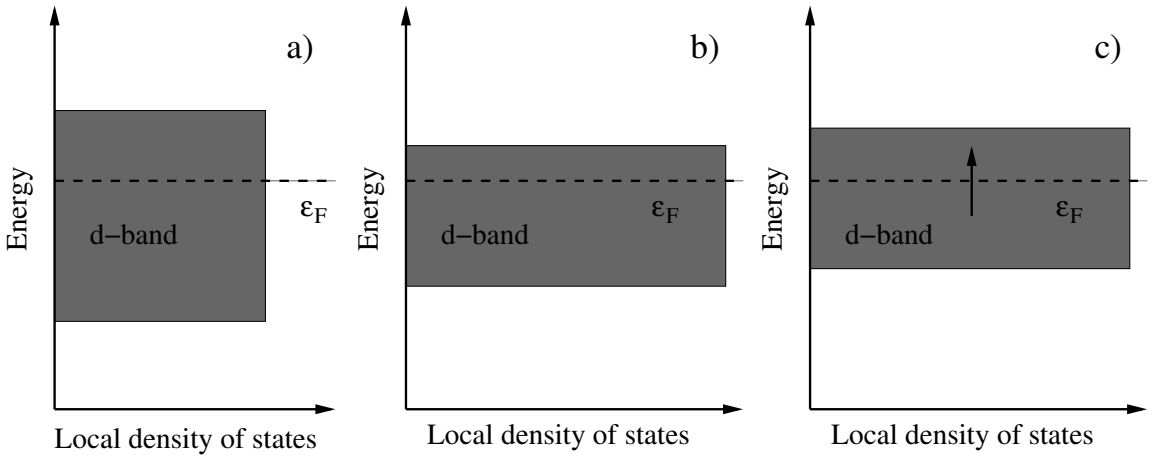

FIG. 3: Illustration of the effect of a lower coordination or smaller atomic overlap on the width and position of a *d*-band. a) *d*-band of a transition metal; b) reduced width of the *d*-band due to a lower coordination or smaller overlap; c) upshift of the *d*-band because of charge conservation.

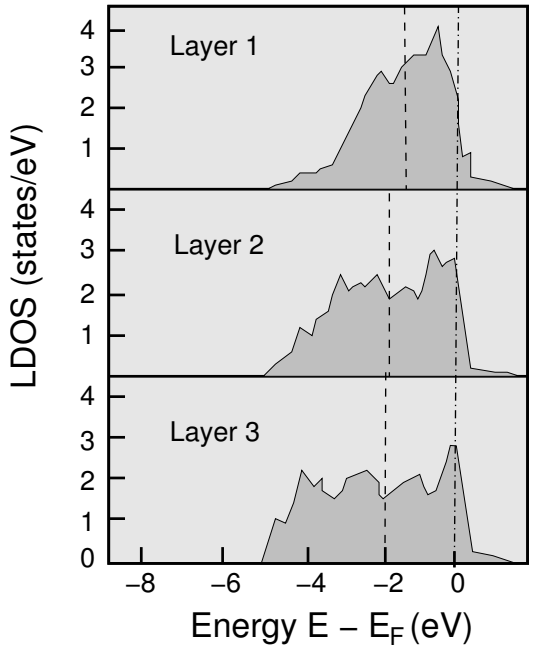

FIG. 4: Layer-resolved, local *d*-band density of states of Pd(210) determined by GGA-DFT calculations. The Fermi level and the center of the *d*-band are indicated by vertical dash-dotted and dashedlines, respectively. The third-layer LDOS is already very close to the bulk density of states of palladium (after [56]).

lead to an higher occupation of the *d*-band. However, the number of *d*-electrons is conserved. In order to obey charge conservation, the narrower *d*-band has to shift up (Fig. 3c) so that the number of occupied states remains unchanged. Thus also the *d*-band center will move up. According to the *d*-band model, this results in a higher reactivity of the structured system.

That the simple concept of the *d*-band upshift due to the band narrowing is indeed true is illustrated in Fig. 4, where the layer-resolved, local *d*-band density of states (LDOS) of the stepped Pd(210) surface determined by GGA-DFT calculations [56] is plotted. The LDOS of the third layer is still rather close to the Pd bulk density of states. This is a consequence of the good screening properties of metals [57] which lead to a rapid recovery of bulk properties in the vicinity of imperfections such as surfaces. However, the width of the *d*-band of the second and first layer are significantly reduced, and this reduction in band width is accompanied by an upshift of the *d*-band centers indicated by the vertical dashed lines. The consequences of this upshift on the interaction strength with adsorbates will be discussed in the next section. Furthermore, it should also be remembered that density of states effect are only related to the band-structure energy. This is, however, only one term in the sum yielding the Kohn-Sham total energy. There are many systems where electrostatic effects or even exchange-correlation effects contribute to the chemical reactivity and interaction strengths.

III. ADSORPTION ON STEPPED SURFACES

Nanostructures at surfaces often exhibit a broad variety of possible adsorption sites because of their open defect-rich structure. This makes a microscopic identification of the relation between the geometric and electronic structure and its reactivity towards adsorption rather complicated. Similarly, the activity of realistic, nanostructured catalysts is often assumed to be dominated by so-called *active sites*, i.e., sites with a specific geometric configuration that modifies their electronic and chemical properties. However, the exact microscopic structure of these active sites is often unknown.

In order to systematically investigate the properties of

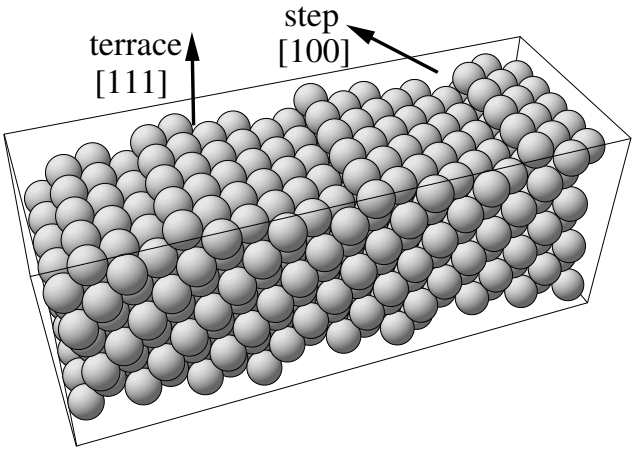

FIG. 5: A stepped (755) = 6(111) × (100) vicinal surface. Steps with ledges of (100) orientations separate (111) terraces that are 6 atom rows wide

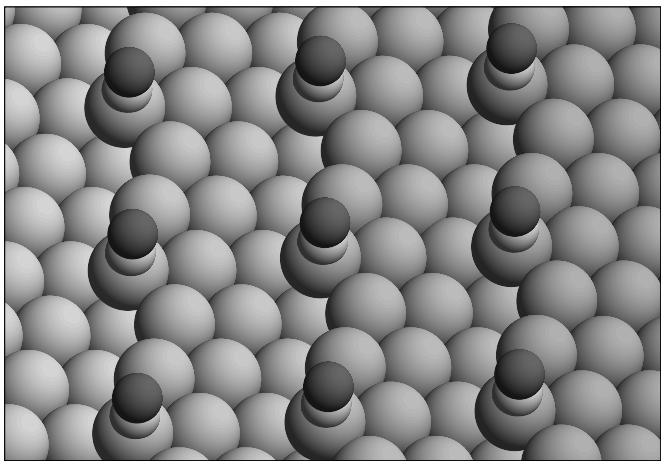

FIG. 6: CO adsorption on top of the kink sites at the steps of a Pt(11 7 5) surface. CO binds with the C end down

nanostructures, it is desirable to prepare surface structures with one well-defined defect structure so that its influence can be isolated from that of all other possible structures. *Vicinal surfaces* are particularly well-suited for this purpose. These are surfaces that are only slightly misaligned from a low index plane. A vicinal surface is structured as a periodic array of terraces of a low-index orientation separated by monoatomic steps. By studying vicinal surfaces, the influence of steps on, e.g., adsorption properties or reactions on surfaces can be studied in a systematic way. They allow to determine the role of steps in the interaction of atoms and molecules with surfaces, they can be relatively easily prepared in the experiment and they are accessible to electronic structure calculations.

In Fig. 5, a (755) surface is shown illustrating the structure of a vicinal surface. The high-index (755) surface consists of 6 atomic rows of (111) orientation separated by a step with a (100) ledge, i.e., the ledge represents (100) microfacets. The misalignment from the [111] direction is 9.5°. In fact, in order to make the structure of a vicinal surfaces immediately obvious, they are often denoted by $n(hkl) \times (h'k'l')$ [58] where (hkl) and $(h'k'l')$ are the Miller indices of the terraces and of the ledges, and n gives the width of the terraces in number of atomic rows parallel to the ledges. Thus a (755) surface is represented by $6(111) \times (100)$. Another example is the $(911) = 5(100) \times (111)$ surface that is rotated by 9.5° from the [100] direction.

Experimentally, it is well-known that many adsorbates bind preferentially to step sites [17, 59]. This has of course motivated electronic structure calculations. A particularly well-studied system is the adsorption of CO on Pt surfaces. Interestingly enough, DFT calculations using present-day functional for the description of the exchange-correlation effects fail in predicting the correct adsorption site for CO/Pt(111) [31]. According to the DFT calculations, the three-fold hollow site is eenrgetically preferred by about 0.25 eV with respect to the top site although it is experimentally well-established that CO adsorbs on the top sites of Pt(111). The reasons for this failure are still debated. Some authors claim that the consideration of relativistic effects leads to the correct site preference. Other claim that the so-called CO/Pt(111) puzzle is caused by the incorrect position of the CO $2\pi^*$ orbital. By correcting its energetic location is an so-called GGA+U approach [60], the true site preference is recovered [61].

However, the system CO/Pt demonstrates that DFT calculations can still be useful and yield important insight into certain aspects of an adsorbate system even if other aspects are not well-described. This is due to the error cancellation in the comparison of similar structures. The binding energies of CO at the on-top sites of several flat, stepped, kinked and reconstructed Pt surface have been invetigated by DFT-GGA calculations [51]. These calculations have revealed a strong structure sensitivity of the binding strength with variations of 1 eV in the CO adsorption energies.

As far as stepped surfaces are concerned, the Pt(211) and Pt(11 7 5) surfaces have been considered. Both surfaces have (111) terraces of similar width, but while the (11 7 5) surface has a open kinked structure along the steps (see Fig. 6), the (211) surface is close-packed along the steps (see Fig. 7). And indeed, the lowest-coordinated Pt atoms which are the kink atoms of the (11 7 5) surface show the strongest binding to CO with bonding energies that are about 0.7 eV stronger than on the flat Pt(111) terrace. These findings have again been rationalized using the d-band model [51]. The lower the coordination, the larger the d-band shift and consequently the higher the adsorption energy.

In this context, it should be mentioned that the Pt(100) surface in equilibrium exhibits a Pt(100)-hex reconstruction which is an otherwise flat (100) surface covered by a hexagonally packed, buckled Pt overlayer. This

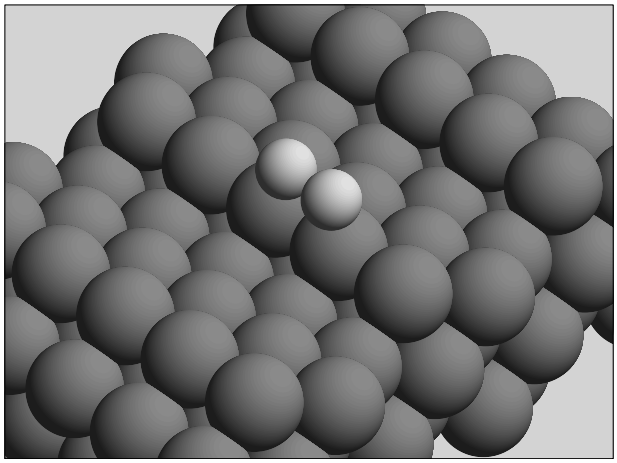

FIG. 7: Molecular O_2 adsorption site at the steps of a Pt(211) surface determined by DFT calculations [17]. For the sake of clarity, the O_2 coverage in the figure does not correspond to the one used in the calculations.

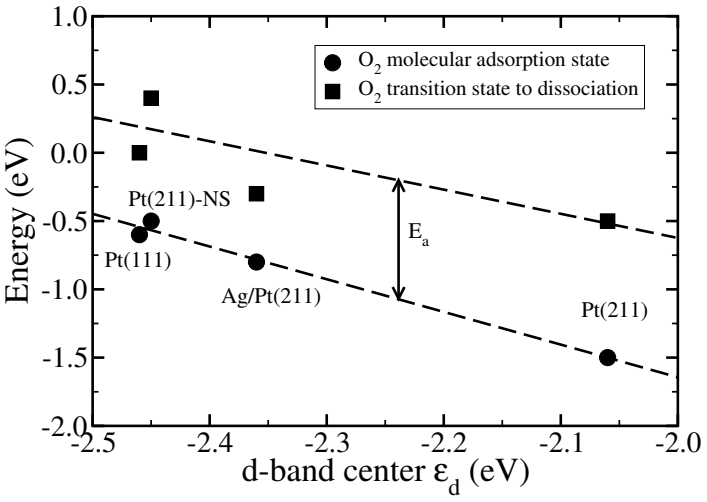

FIG. 8: O_2 molecular adsorption energy and transition state energies determined using the GGA-PW91 functional as a function of the local d-band center ε_d [71]. The dashed lines are included as a guide to the eye.

overlayer is buckled because the Pt density in the overlayer is 4% higher than in the Pt(111) surface. This larger density has the same effect as a higher coordination. Because of the increased overlap the d-band broadens and shifts to lower energies making it less reactive. This is exactly what has been found for the binding of CO on the Pt(100)-hex(1×5) surface which is weaker by 0.1 eV compared to the Pt(111) surface.

Apart from the CO/Pt system, the interaction of molecular oxygen with Pt surfaces represents one of the best studied systems in surface science, both experimentally [62–67] as well as theoretically [68–70]. This interest, as for CO/Pt, was also motivated by the technological relevance of the adsorption of O_2 on Pt as a crucial microscopic reaction step occuring in the car-exhaust catalyst. O_2 can adsorb both molecularly and dissociatively on Pt. At surface temperatures below 160 K O_2 only adsorbs molecularly because of steric hindrances [70], even if the molecules impinge on the surface with high kinetic energies [64].

Experimentally, it has been found that the O_2 dissociation is strongly favored at step sites [17]. The local reactivity of the Pt step sites is reduced significantly when the step sites are decorated by Ag atoms. In the experiment, two vicinal surfaces were studied, Pt[9(111)×(111)] and Pt[8(111) × (100)], which have both (111) terraces that are nine and eight atom rows wide, separated by {111} and {100} monatomic steps, respectively. In order to understand the enhanced reactivity of the Pt steps, GGA-DFT calculations have been performed [17, 71]. In the calculations, O_2 adsorption and dissociation on Pt(211)=Pt[3(111)×(100)] were addressed. The terraces of this surface are only three atom rows wide. Still, the steps of the (211) are far enough from each other to make the calculations relevant for the understanding of the reactivity of the vicinal surfaces studied in the experiments.

In the calculations, the O_2 molecular adsorption state and its energy $E_{\rm mol}$ and the energy of the transition state to dissociation $E_{\rm TS}$ were determined for the step site and a "near step" (NS) site one row away from the steps of the clean Pt(211) surface and for the Pt(211) surface with the steps decorated by a monatomic row of silver atoms. The energetically most favorable molecular adsorption state of O_2 on Pt(211) which is shown in Fig. 7 is indeed at the Pt step atoms. The same is true for oxygen atoms which also preferentially adsorb at the Pt step atoms [23]. In passing I note that in order to illustrate both the surface geometry and the adsorbate location, in Fig. 7, as in many of the following figures, only a single adsorbed molecule has been plotted. However, one has to keep im mind that the coverages used in the calculations within the supercell approach are usually much higher.

The stronger binding to the steps can again be understood within the d-band model. In Fig. 8, the O_2 adsorption and transition state energies are compared to the corresponding ones for the Pt(111) surface as a function of the local local d-band center ε_d. These energies were determined using both the RPBE and the PW91 functional, but only the PW91 results are plotted in Fig. 8 since the qualitative consequences do not depend on the functional. The correlation between the energies and the position of ε_d is obvious. At the step sites, the low coordination leads to a upshift of the d-band center which results in a stronger interaction.

Interestingly enough, the local barrier for dissociation $E_a = E_{\rm TS} - E_{\rm mol}$ is not lowered at the steps. There, it is even higher than on the flat Pt(111) surface. Thus it seems to be surprising that there is a higher rate for dissociation at the steps. However, not only the height of the local dissociation barrier, but also the absolute energetic position of the transition state with respect to the O_2 molecule in the gas phase are important. At the

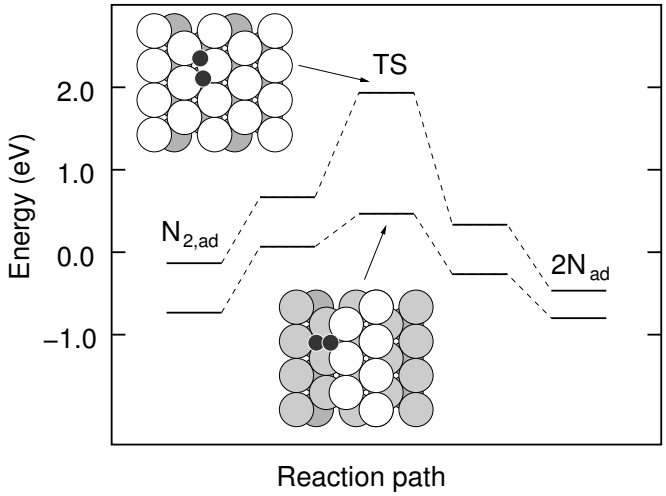

FIG. 9: Energetics of the N_2 dissociaton on a terrace and a step of Ru(0001) as determined by DFT calculations [72]. The insets show the corresponding configurations at the transition state (TS) for dissociation. The energy zero is chosen to be the energy of the N_2 molecule in the gas phase.

flat Pt(111) surface, the transition state energy approximately coincides with the energy of O_2 in the gas phase which means that the energetic heights of the dissociation barrier and the desorption barrier are similar. Hence, in a thermally activated situation, a large fraction of adsorbed oxygen molecules will rather desorb than dissociate. At the steps, where the transition state energy is well below the O_2 gas phase energy, the branching ratio between dissociation and desorption is strongly shifted towards dissociation although the absolute value of the barrier is higher at the steps. Hence, it is the stabilisation of the molecular adsorption state that leads to an enhanced dissociation at steps.

Steps do not only provide sites for preferential adsorption, they could also lead to the lowering of reaction barriers. One important example is the N_2 dissociation on the Ru(0001) surface which has been shown experimentally to be totally dominated by steps [72, 73]. This system is of particular importance since the N_2 dissociation represents the first and rate-limiting step in the ammonia synthesis [74, 75]. The experimentalists have again used the fact that Au atoms deposited on a Ru(0001) surface will preferentially decorate the steps thus blocking these sites [59]. The Ru(0001) surface used in the experiments had a step density of less than 1%. By depositing less than 2% of a monolayer of gold the N_2 dissociation rate was suppressed significantly. From the experimentally measured rates it was estimated that the dissociation rate at the steps is at least nine orders of magnitude higher than on the terraces at 500 K [72, 73].

Theoretically, the N_2 dissoication on Ru(0001) surface was described within a (2×2) surface unit cell [72, 76]. The step was modeled by using a (2×4) unit cell and removing two rows of Ru atoms (see inset of Fig. 9). The energetics along the reaction path from the molecular N_2 precursor state to atomic nitrogen on the surface is also shown in Fig. 9. It is obvious that the barrier for the dissociative adsorption of N_2 is significantly lowered from 1.9 eV at the terraces to 0.4 eV at the steps, in agreement with the experiment. While the N_2 molecular precursor is also strongly stabilized at the steps, the difference in the binding energies of atomic nitrogen at the steps and the terraces is much smaller. For the N_2 dissociation this is important because it means that the nitrogen atoms after dissociation do not block the step sites so that they can act as a low barrier channel for populating the terraces.

At first sight, the transition state configurations on the terrace and at the step are not too different. In both cases, one nitrogen atom is close to the most stable hcp site while the other is located at a bridge position. However, at the step the two N atoms do not share any Ru atoms as nearest neighbors. This reduces the indirect repulsive interactions that lead to the high N_2 dissociation barrier on the terrace [77]. Hence it is the modified geometrical arrangement of the steps that contributes significantly to the higher reactivity. In a subsequent theoretical study, it was shown that also for the ammonia synthesis over a Ru surface the reactions mainly take place at the step sites [76].

Furthermore, a dramatic lowering of the dissociation barrier at stepped ruthenium surfaces does not only occur for N_2, but also for NO. DFT calculations found that this barrier is reduced from 1.28 eV at the flat Ru(0001) surface to 0.17 eV at a stepped Ru surface [78]. These results agree with the experimental findings of a STM study that NO dissociation only occurs at the steps of a vicinal Ru surface [79]. This strong reduction is caused by so-called final state effects. First, the reaction products, atomic nitrogen and oxygen are more strongly bound at the steps than on the terrace, and second, at the steps the reaction products share less nearest neighbor surface atoms, as in the case of N_2 dissociation. This again shows that the modified structural arrrangement at the steps plays a very important role for their reactivity.

Stepped surfaces do not only lead to a stronger interaction with adsorbates because of the lower coordination of the step atoms, they can also induce unusual adsorption structures, such as the stabilization of a molecular state by the presence of atomic adsorbates. Hydrogen molecules usually adsorbs dissociatively at metal surfaces [80], not molecularly. Molecularly chemisorbed H_2 species have only been found at stepped metal surfaces. On Ni(510), a molecular adsorption state at surface temperatures up to 125 K has been observed at the step sites, but only after the surface was passivated with a dense atomic hydrogen layer [81]. On Cu(510), a weakly bound species has been observed at low temperatures on the clean surface [82, 83].

On Pd(210), experiments have found the coexistence of chemisorbed hydrogen atoms and molecules on Pd(210) which was deduced from isotope exchange experiments [84]. The microscopic nature of the adsor-

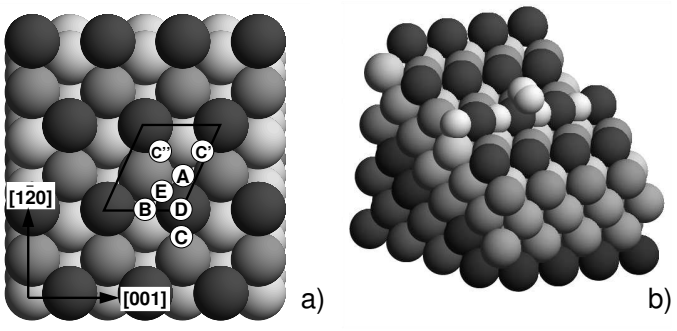

FIG. 10: Structure of the Pd(210) surface. a) Top view of the (210) surface together with the surface unit cell and CO and H adsorption sites; b) one row of adsorbed hydrogen atoms at the open (110)-like microfacets is shown. Once these bridge sites are occupied by hydrogen atoms, a H_2 molecular chemisorption state becomes stabilized above the Pd step atoms [56, 84].

TABLE I: Atomic hydrogen binding energies in eV/atom and CO binding energies in eV/molecule on clean Pd(210) for fixed and relaxed slabs. For the site assignment, see Fig. 10a. For hydrogen, also the octrahedral subsurface site O_d has been considered. For the coadsorption system, the listed binding energies correspond to atomic H adsorption on the CO-precovered Pd(210) surface. The coverage corresponds to one H atom and one CO molecule per (210) surface unit cell [56, 89].

		$E_{\rm ad}$ (eV)	
CO-pos	H-pos	Fixed slab	Relaxed slab
–	A	–	0.45
–	B	–	0.52
–	C'	–	0.51
–	O_d	–	0.21
E	–	1.83	1.88
C	–	1.76	1.86
B	–	1.73	1.77
E	A	0.09	0.12
E	C'	0.22	0.31
E	C"	0.19	0.27
C	A	0.13	0.22
C	B	0.24	0.30

bate states, however, could not be clarified from the experimental information. On the low-index Pd surfaces, it is well-accepted that hydrogen only adsorbs dissociatively [85, 86].

The hydrogen/palladium system has in fact been a model system for the study of the interaction of hydrogen with metal surfaces [87] which was also caused by the potential role of palladium as a hydrogen storage material. In order to identify the microscopic nature of the molecular H_2 adsorption state on Pd(210), DFT-GGA calculations have been performed [56, 84] using the Perdew-Wang functional (PW91) [33]. The geometry of the (210) surface plus the surface unit cell is shown in Fig. 10a in a top view. In addition, possible adsorption sites are labeled. The (210) surface can be regarded as a stepped surface with a high density of steps [88]. Vicinal fcc(n10) surfaces have (100) terraces with steps running along the [001] direction. These steps are forming open (110)-like microfacets.

The calculated hydrogen binding energies on Pd(210) are listed in table I. The long-bridge position between two Pd step atoms (site B) corresponds in fact to the most favourable adsorption site for atomic hydrogen , as indicated in Fig. 10b, although usually hydrogen prefers highly-coordinated adsorption sites at metal surfaces [80]. This preferential adsorption on the low-coordinated step sites can be traced back to the upshift of the local d-band center at these first layer atoms (see Fig. 4). However, the long-bridge position is practically degenerate with the quasi-threefold position C' on the level of accuracy of the DFT calculations, as Table I indicates. In spite of the fact that there is mutual repulsion between the adsorption hydrogen atoms on Pd(210), still two additional hydrogen atoms can be adsorbed within the (210) surface unit cell at terrace sites A and C [56, 84].

On the clean Pd(210) surface, H_2 dissociates spontaneously without any hindering adsorption barrier, like on the low-index palladium surfaces [85, 90, 91]. However, once the long-bridge sites at the steps are occupied by hydrogen atoms, a barrier for the dissociative adsorption builds up although hydrogen adsorption is still exothermic. This hydrogen precoverage leads to a metastable H_2 molecular chemisorption state above the Pd step atoms with a binding energy of 0.27 eV [56, 84]. This molecular state is also illustrated in Fig. 10. The preadsorbed atomic hydrogen does not significantly disturb the interaction of the H_2 molecules with the step Pd atoms but hinders the H_2 dissociation on Pd(210). In fact, the molecular adsorption state corresponds locally to the stable PdH_2 complex found in the gas-phase [92, 93]. This unique feature of a nanostructured surfaces might be useful for catalyzing certain reactions in which, e.g., relatively weakly bound hydrogen molecules are required.

Palladium is known to be able to absorb large amounts of hydrogen which is important in the context of hydrogen storage and technology [94]. Therefore the subsurface absorption as the first step for the hydrogen dissolution into the bulk is also of particular interest. The binding energy of hydrogen in the octahedral subsurface site is 0.21 eV (see Table I), i.e. significantly lower than on the surface. This means that hydrogen prefers to stay on the surface. Only if the surface is fully covered with hydrogen, absorption into the bulk starts [84]. Furthermore, the hydrogen subsurface binding energies at the open Pd(210) surface and at the low-index Pd(111), Pd(111) and Pd(110) are basically the same. The open structure of the steps does apparently not play a significant role in the subsurface absorption. Because of the small size of the hydrogen atom, the substrate relaxations

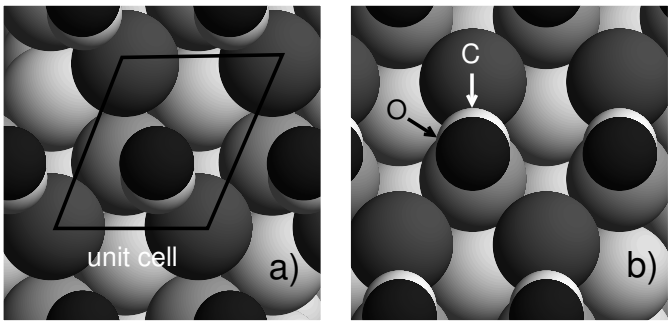

FIG. 11: Adsorption geometries for CO on Pd(210), a) at site E, and b) at site B. O is drawn in black, C in white, the Pd atoms are shaded in gray. In both cases, the bridge-bonded, inclined CO geometry is clearly visible.

induced by the hydrogen subsurface absorption are only relatively small and limited to the first layer [56].

In addition, the CO adsorption on Pd(210) was addressed by DFT calculations [89]. Interestingly, CO does not preferentially bind to the step sites B, as Table I shows, but rather to the bridge sites E and B which are energetically degenerate according to the DFT calculations. The local bonding geometry of CO at these sites is shown in Fig. 11. These results can be understood considering the fact that CO is known to occupy bridge sites on Pd(100) [95, 96] and near-bridge sites on Pd(110) [97–99]: site E corresponds to a bridge position on the (100) terrace, site C to a bridge position on a (110) facet. It is furthermore obvious from table I that relaxation effects of the substrate are indeed not negligible for the adsorption at the open Pd(210) surface.

As far as the CO adsorption site is concerned, the DFT calculations are in agreement with electron stimulated desorption ion angular distribution (ESDIAD) measurements [100] at low coverages up to $\theta = 1$ which suggest CO adsorbs in a bridge-bonded position at site E, inclined away from the surface normal. Thermal desorption results yield an initial adsorption energy of 1.52 eV [101] or 1.45 eV per CO molecule [102]. Thus the calculated CO binding energies on Pd(210) seem to be overestimated. This is a well-known phenomenon, GGA calculations using the PW91 exchange-correlation functional tend to overestimate the CO adsorption on a wide range of metal surfaces [103].

On Pd(100), the CO adsorption energy is 1.91 eV at the bridge position for the $c(2\sqrt{2} \times \sqrt{2})$ CO superstructure, in good agreement with other calculations using a slightly different setup [96]. However, this means that the adsorption energy of CO on Pd(210) is slightly lower than on Pd(100). Experimental TDS results, too, suggest a slightly higher adsorption energy on Pd(100) than on Pd(210) [101]. Considering the low coordination of the top Pd atom and thus its high reactivity, it might have been anticipated that CO would actually be more strongly bound to the stepped Pd(210) surface. For example, on stepped Pd(211) and Pd(311)-missing-row surfaces, the CO binding energies are larger than on Pd(100) and Pd(111) according to DFT calculations [104]. For the on-top site of Pd(210), this is indeed true: adsorption at site D gives a binding energy of 1.50 eV, whereas on-top adsorption on Pd(100) gives 1.44 eV [96].

The reduced binding energy of CO at the bridge sites of Pd(210) can be understood if the local bonding geometry is considered. Adsorption in both bridge-bonded sites results in rather strong relaxations. Furthermore, a tendency to minimize the CO inclination has been found. This indicates that the CO molecule is repelled by the protruding Pd atom at the next "step". Adsorption is thus not as favorable as on a flat (100) surface where there is no adjacent repelling Pd atom. In addition, the variations in the tCO adsorption energy from site to site are comparably small. Hence, a rather small energy gain due to a more reactive bonding partner might just be overcompensated by the enforced, but unfavorable inclination of the molecule.

Furthermore, the coadsorption of CO and hydrogen on Pd(210) was studied by the DFT calculations [89]. Experiments of CO and H_2 adsorption showed a strong inhibition of hydrogen adsorption in the presence of CO on Pd(210) [102]. Coadsorption studies involving CO are of great technological relevance since CO is known as a rather unwanted catalytic poison. Since it binds rather strongly ($\approx 1 - 2$ eV) to many metal surfaces, it is able to passivate an otherwise reactive surface by just blocking the sites at which the wanted reaction would occur [105]. However, coadsorption studies are not only of interest in the context of the poisoning of a catalyst. In general, any heterogeneously catalyzed reaction requires the coadsorption of the reactants, thus confirming the importance of a fundamental insight into the interaction between two adsorbed species.

The computed atomic hydrogen adsorption energies for one hydrogen atom per surface unit cell in the presence of CO at different sites are also listed in table I. The overall trend is a significant reduction of atomic hydrogen adsorption energies at all sites due to the presence of CO on Pd(210), in agreement with the experimental results [102]. This reduction might be caused by a direct mutual electrostatic repulsion. Both atomic hydrogen and CO lead to an increase of the work function upon adsorption which means that they should experience a mutual dipole-dipole repulsion when they are coadsorbed. However, the increase of the work function upon atomic hydrogen adsorption is rather small, about 0.2 eV [84]. Furthermore, atomic hydrogen is adsorbed much closer to the surface than CO. Both facts indicate that the dipole-dipole interaction between adsorbed CO and H should be small.

Apart from the direct interaction between the coadsorbates, the CO-induced modification of the substrate density of states can also lead to significant changes in the hydrogen adsorption energies, as for example found in the case of the poisoning of hydrogen dissociation at Pd(100) by adsorbed sulfur [22, 106]. Upon CO adsorption, the

local d-band center at the top Pd atom is shifted down significantly from $\varepsilon_d = -1.26$ eV at the clean surface to $\varepsilon_d = -1.82$ eV. This considerable downshift is caused by the strong interaction of CO with Pd and is much larger than the corresponding value for H adsorption on Pd(210). As mentioned above, an energetic downshift of the position of the local d-band center leads to smaller chemical binding at the particular surface according to the d-band model [47]. This explains the rather large decrease in the hydrogen binding energies on the CO-covered surface.

The adsorption on (n10) surfaces was also the subject of a number of experimental and theoretical studies for the O/Ag system. Using molecular beam techniques and high-resolution electron energy loss spectroscopy (HREELS), Rocca and coworkers found that the steps of the Ag(210) and Ag(410) surface represent the active sites for the dissociative adsorption of O_2 while the oxygen atoms adsorb at different sites [107–109].

Motivated by these experimental investigations, the identification of the most stable atomic oxygen adsorption sites on Ag(210) and Ag(410) was addressed in a DFT study [110]. The results with respect to the binding energies of the oxygen atoms at step (S) and terrace (T) sites are summarized in table II. The given coverage θ_O is related to the number of oxygen atoms per surface unit cell. At the Ag(210) surface, the adsorption at the step sites is preferred compared to the terrace sites, as for H/Pd(210) [56], while on Ag(410) the adsorption energies are very similar at the step and the terrace sites. The subsurface incorporation of oxygen at the octahedral site of Ag(210) is energetically much less favorable than oxygen adsorption on the surface, again similar to H/Pd(210), but here it is mainly caused by the strong lattice distortion upon oxygen subsurface absorption [111].

The most peculiar result, however, is the increased stability of the oxygen atoms when they fully decorate the steps in a (1×1) geometry. This is in fact surprising because the negatively charged oxygen atoms experience a electrostatic repulsive interaction. For example, on Pt(211) where oxygen atoms also bind preferentially to the step sites, the (2×1) structure is more stable by 0.48 eV/adatom compared to the (1×1) structure [23] where every other step site is occupied.

The structure of oxygen atoms adsorbed in a (2×1) and a (1×1) structure at the step sites of a Ag(410) surface is illustrated in Fig. 12. First of all, it is obvious that the oxygen atoms are almost at the same height as the adjacent Ag atoms which means that they are effectively screened from each other by the Ag step atoms. However, this alone can not explain the higher stability of the fully decorated steps. In fact, the authors of the computational study [110] do not have a water-proof explanation for this phenomenon. They believe that the mechanism causing this stability could be related to the arrangement of the O adatoms in O-Ag-O chains at the upper sides of the (110) steps. Such chains are for example also found in the added-row reconstruction of Ag(110) upon oxygen adsorption [112].

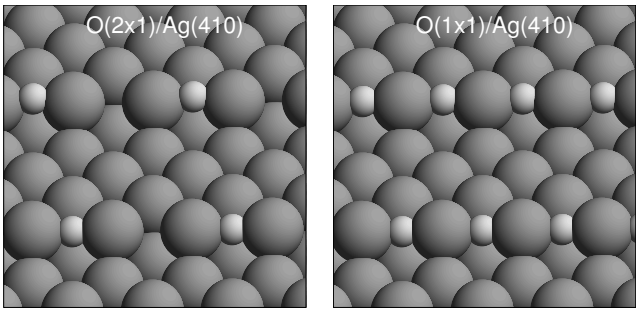

FIG. 12: Optimized geometries of oxygen atoms adsorbed in a (2×1) and a (1×1) structure at the step sites of a Ag(410) surface [110].

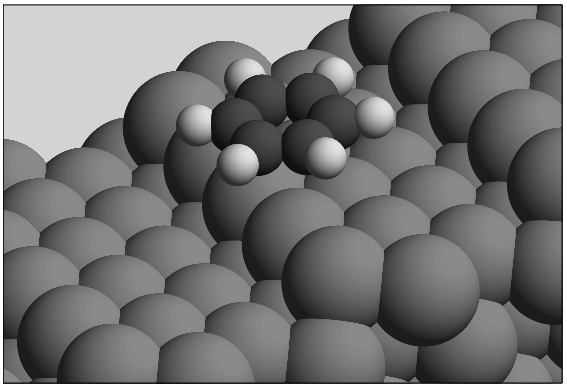

FIG. 13: Optimized structure of benzene, C_6H_6, adsorbed above a stepped Ni(221) surface according to DFT calculations [113]. The center of mass of the benzene molecule is shifted by about 1.0 Å from the step edge.

As far as the oxygen position in the (2×1) and the (1×1) structures are concerned, for the high coverage the oxygen atoms are even closer to the surface than for the low coverage. Thus the Ag and O are almost aligned at the same height. Although there is some hybridization between the oxygen and the silver electronic states, there is a significant charge transfer only from the silver atoms at the steps to the oxygen atoms, leading to a electrostatically stable chain of atoms with alternating charges in the (1×1) structures. Interestingly enough, in the (2×1) structure the charge transfer from the terrace atom to the oxygen atom is very similar to the transfer from the step atoms. Hence, the electrostatic rearrangement is not restricted to the step atoms. Certainly, the stability of the oxygen-decorated Ag steps deserves further investigations.

The molecules treated in the studies discussed above were relatively simple. However, the interaction of organic molecules with nanostructured surfaces is of course also very relevant in the field of heterogeneous catalysis [114]. In a DFT study, it was shown that there is also a considerable influence of steps on the adsorption

	E_b(eV)				
surface	S, $\theta_O = 1/2$	T, $\theta_O = 1/2$	S, $\theta_O = 1$	T, $\theta_O = 1$	O_d, $\theta_O = 1/2$
Ag(210)	0.68	0.49	0.80	0.42	0.07
Ag(410)	0.75	0.80	0.86	0.79	–

TABLE II: Binding energy of oxygen atoms in eV/atom on Ag(210) and Ag(410) at step (S) and terrace (T) sites [110] and at the octahedral subsurface site O_d [111]. The coverage θ is related to the number of oxygen atoms per surface unit cell.

of benzene on nickel [113]. Several adsorption positions of the benzene molecule which corresponds to an aromatic π electron system with respect to the step edge have been considered. The most stable adsorption position of benzene is illustrated in Fig. 13. The center of mass of the carbon rings is situated 1.0 Å away from the step edge. At this site, the binding energy of benzene, $E_b = 1.37$ eV, is enhanced by about 0.3 eV with respect to the value for the flat surface, $E_b = 1.05$ eV, and also with respect to the one for the center of mass of the benzene directly above the step edge.

Benzene binds to the nickel surface by forming bonds between the carbon and the metal atoms. The hydrogen atoms are rotated slightly upwards indicating a repulsive interaction between the hydrogen and the nickel substrate. This interpretation is supported by the fact that the binding energy of benzene to Ni(221) is further decreased by another 0.3 eV if the benzene molecule is shifted close to the step edge from below so that the hydrogen atoms interact with the Ni step atoms. The energetically most favorable adsorption position near the step allows the creation of strong bonds between the carbon ring and several nickel atoms. However, a shift of the molecule parallel to the surface hardly affects the binding energies. This seems to indicate that it is not the local bonding configuration at the step but rather the specific electronic properties of the step that cause its higher reactivity. And indeed, an analysis of the electronic structure shows that the polarization effects are larger at the steps which leads to a larger charge transfer from the Ni atoms to the bonding region and thus to stronger bonds [113].

A similar enhancement of the binding energies at the steps of a metallic surface has also been found in DFT calculations addressing the adsorption of ethylene, C_2H_4, on Ag surfaces [115, 116]. While ethylene hardly binds at the flat Ag(001) surfaces, the binding energy at the step sites of a Ag(410) is 0.25 eV. This stronger binding, however, has been attrributed to the enhanced hybridization between the silver d and the ethylene π^* states at the steps.

The issue of chirality and so-called stereoselectivity of organic molecules on stepped surfaces had been addressed in a very ambitious DFT study [117]. High-index surfaces of fcc crystal with kink sites at the steps lack symmetry apart from translational symmetry when the step lengths or step faces on the two sides of the kink are not equal [118]. Two such surfaces which are created by reflection can not be superimposed on each other, and the kink sites are either left- or right-handed, i.e. they are

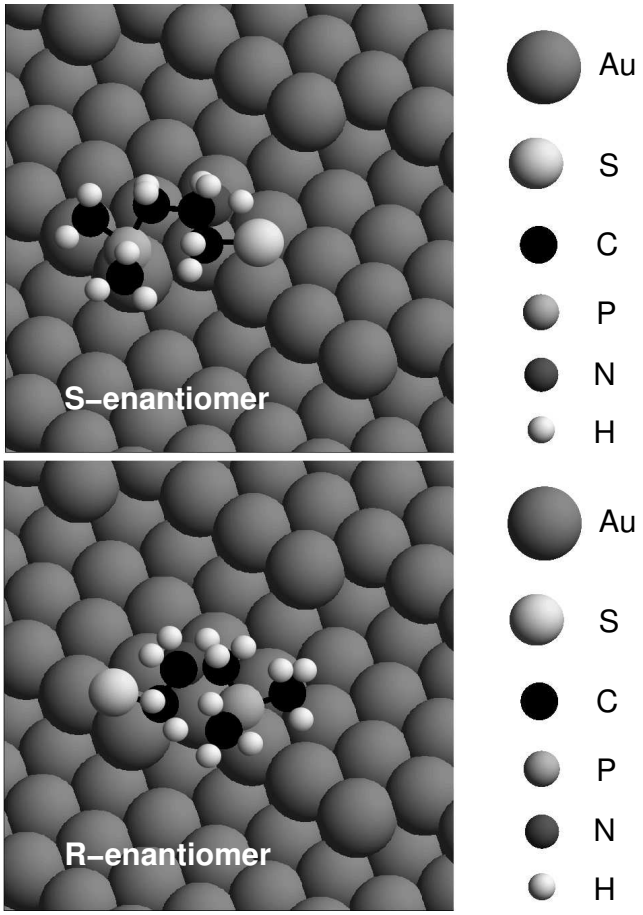

FIG. 14: Most stable adsorption configurations for the S-enantiomer and the R-entantiomer of APPT on Au(17 11 9)^S as determined in DFT-GGA calculations (after [117]).

chiral. One example of such a surface is the (643) surface, another one is the (17 11 9) surface which is illustrated in Fig. 14. In fact, in Fig. 14 the $(17\,11\,9)^S = (\bar{1}7\,11\,9)$ surface is shown whereas the $(17\,11\,9)^R = (17\,11\,9)$ is its enantiomorph that possesses the opposite chirality.

The chirality of organic molecules is actually rather important for molecular recognition and interaction. And the existence of chirality in kinked single crystal metal surfaces suggests that the adsorption and reaction probabilities of chiral molecules on these surfaces should be stereoselective, i.e. they should depend on the chirality of the molecules. Indeed, such a selectivity has been found, for example in the interaction of glucose with

Pt(643) [119].

The first DFT study of the adsorption of a chiral molecule on a chiral surface was performed for the S and R enantiomers of 2-amino-3-(dimethylphosphino)-1-propanethiol (APPT, $HSCH_2CHNH_2CH_2P(CH_3)_2$) on $Au(17\,11\,9)^S$ [120]. This particular molecule was chosen because in previous studies it was shown that their thiolate, phosphino, and amino groups are all able to bind to gold surfaces [121, 122]. The two most stable adsorption sites of the S and R enantiomers of ATTP on $Au(17\,11\,9)^S$ are shown in Fig. 14. Their binding energies are 0.9 eV and 0.8 eV, respectively, i.e. there is an enantiospecifity in their binding. A closer analysis shows that in the enenergetically most favorable configurations ATTP binds indeed with its thiolate, phosphino, and amino groups to the gold atoms. By performing model calculations for the three groups alone it was shown that the binding of ATTP to $Au(17\,11\,9)^S$ can be understood in terms of these three local bonds plus the deformation energies of the molecule and the surface, respectively.

In the most favorable binding configurations, the molecular deformation is rather small. The enantiospecific binding rather results from the ability or inability to simultaneously optimize three local bonds. While the S-enantiomer of ATTP is able to find such an optimal adsorption configuration, the R-enantiomer is less favored since it is not capable of optimizing neither the thiolate-gold nor the amino-gold bonds. This fits into the picture that chiral recognition might be in general driven by the formation of three-point contacts [123] which represent the smallest number of contact points able to discriminate between two different enantiomers.

Interestingly enough, for two other related chiral molecules, the naturally occuring amino acid cysteine ($HSCH_2CHNH_2COOH$) and 2,3-diamino-1-propanethiol (DAPT, $HSCH_2CHNH_2CH_2NH_2$), no enantiospecific binding was found. For cysteine the lack of stereoselectivity in the adsorption on $Au(17\,11\,9)^S$ is caused by the fact that it only binds on $Au(17\,11\,9)^S$ through two groups, its thiolate and amino groups. DAPT, however, has three groups that all form bonds with the surface, but two of them, the amino groups, are equal. Thus it is apparently important for the chiral behavior that all three molecule-surface bonds are different. This suggests that the character of the functional group mediating the binding is crucial for enantiospecific behavior.

So far, we have exclusively considered the adsorption of atoms and molecules on stepped *metal* surfaces. However, semiconductor surfaces are also of considerable technological importance, in particular Si surfaces, in the context of information technology. Especially the H_2/Si system has attracted a lot of attention [124] since hydrogen adsorption leads to a passivation of the surface. Furthermore, hydrogen desorption is the rate determining step in the growth of silicon wafers from the chemical vapour deposition (CVD) of silane.

On the flat Si(100) surface, the dissociative adsorption of H_2 is hindered by a barrier of the order of 0.4 eV according to DFT slab calculations [125, 126], although the exact value of this barrier is still debated [127]. However, it was found experimentally that the hydrogen sticking coefficient at steps of vicinal Si(100) surfaces is up to six orders of magnitude higher than on the flat terraces [128].

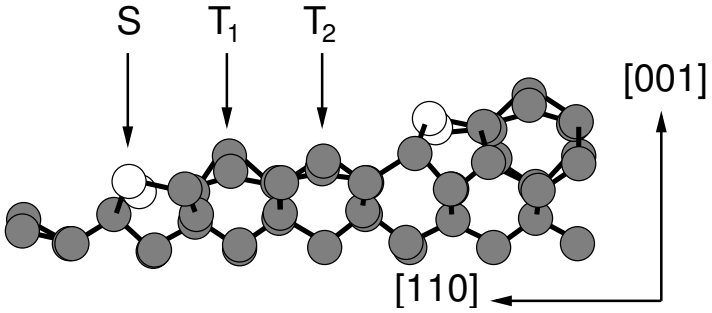

FIG. 15: Relaxed structure of the Si(117) surface with rebonded D_B steps. The rebonded Si atoms are shown in white (after [128]). The step and terrace atoms are denoted by S and T, respectively.

As far as stepped semiconductor surfaces are concerned, it is important to realize that the termination of semiconductor surfaces is usually much more complicated than those of metal surface. This is caused by the covalent nature of the interaction which strongly favors directional bonding and leads to extended reconstruction patterns [16]. At the conditions of the experiment, vicinal Si(100) surfaces have steps with a double-atomic height, the so-called rebonded D_B steps, which have additional coordinated Si atoms attached to the steps [129]. To model the vicinal substrate, a Si(117) surface was used in the calculations [128, 130]. Its structure is shown in Fig. 15 where the rebonded Si atoms are shown in white. These calculations found that hydrogen atoms preferentially adsorb at the steps of the silicon surface. These sites are favored by about 0.1 eV with respect to the terrace sites, which is in fact also true for a Si surface with so-called rebonded single atomic height S_A and S_B steps [130].

However, the influence of the steps on the H_2 dissociation barrier is much more dramatic. While this barrier is 0.40 eV and 0.54 eV at the terrace sites T_1 and T_2, respectively, there is no barrier for dissociation for the H_2 molecule approaching with an orientation parallel to the steps and the two H atoms dissociating towards the Si rebonded atoms [128]. The dissociation process, however, involves some relaxation of the Si atoms with the asymmetry of two adjacent rebonded Si atoms caused by a Jahn-Teller-like like splitting being lifted.

The high reactivity of the steps with respect to H_2 dissociation has been explained by the modification of the electronic structure at the steps. On the flat Si(100) surface, there are two surface bands formed from the dangling bonds located at the Si dimer atoms which are split by approximately 1 eV due to a Jahn-Teller mechanism [131, 132]. The same splitting is observed for the rebonded Si atoms at the steps, as just mentioned above.

However, when the rebonded Si atoms are forced to the same geometric height, the splitting is reduced to 0.4 eV, and the surface states can interact efficiently with the molecular orbitals of the H_2 molecules. At the flat Si(001) surface, the π interaction of the dangling bonds prevents the two surface bands from coming closer to each other which makes the terrace sites less capable of breaking the H-H bond.

Interestingly enough, adsorbates can have a similar effect on the dissociation probability on Si as steps since the electronic structure of the dangling bonds is perturbed in a similar way by both steps and adsorbates [133]. Recent scanning tunneling microscope (STM) experiments demonstrated that predosing the Si(100) surface by *atomic* hydrogen creates active sites at which the H_2 adsorption is considerably facilitated [134, 135]. This confirms that it is often the modified electronic structure that is crucial for the understanding of the chemical properties of nanostructured surfaces. Furthermore, these findings have finally resolved the so-called barrier puzzle for the H_2/Si system [126, 136]: While the sticking coefficient of molecular hydrogen on Si surfaces is very small [137, 138] indicating a high barrier to adsorption, the low mean kinetic energy of desorbed molecules [139] suggests a small adsorption barrier. This puzzle arises from the fact that adsorption experiments are usually performed in the low-coverage regime while desorption experiments are carried out in the high-coverage regime, and for the system H_2/Si the hydrogen coverage has a crucial influence on the adsorption barrier heights.

IV. ADSORPTION ON SUPPORTED CLUSTERS

Clusters are particles with sizes typically between a few and several thousands of atoms. They are characterized by the reduced dimension of the particle, a large surface to volume ratio and a large number of low-coordinated atoms at edge sites. The properties of clusters lie usually between those of single atoms or molecules and those of bulk material. However, often small particles or clusters in the nanometer range show surprisingly strongly modified electronical, optical and chemical properties which can be characterized by saying that small is different [140]. Yet, it is often not clear whether the specific properties are caused by the reduced dimension of the particles ("quantum size effects") or by the large surface area of the nanocluster where many low-coordinated atoms or defects are present.

Free clusters are usually studied in molecular beam apparatuses. For technological applications, free clusters are in general not very useful; they rather have to be fixed in space, either in a bulk matrix as for example the so-called nanodots or quantum dots in semiconductor technology, or on a surface. For these embedded or supported clusters, the interaction with the environment has to be taken into account. In fact, for metal clusters on

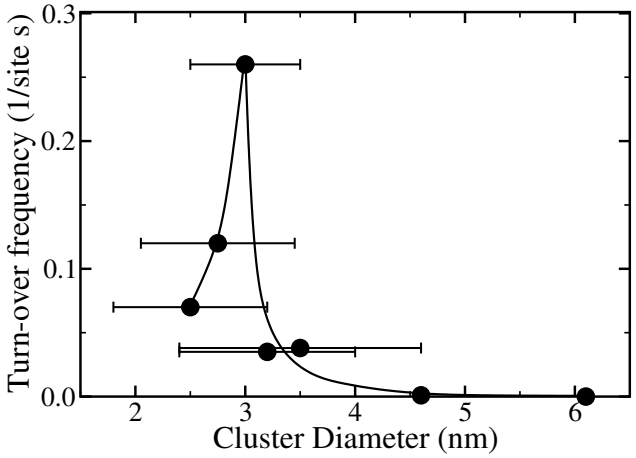

FIG. 16: Measured CO oxidation turnover frequencies at 300 K as a function of the average size of Au clusters supported on a high surface TiO_2 support. The solid line is meant as a guide to the eye (after [18]).

surfaces the so-called strong metal support interaction (SMSI) has been discussed intensively [141, 142] which significantly influences the catalytic properties of group VIII metals such as Fe, Ni, Rh, Pt, Pd, and Ir supported on metal oxides.

In recent years, supported gold clusters have become the prototype system for the study and understanding of the modified chemical properties of nanoscale structures. While gold as a bulk material is chemically inert, mainly due to its energetically low-lying, completely filled d band [48], small Au clusters show a surprisingly high catalytic activity, especially for the low-temperature oxidation of CO [18, 24], but also for NO oxidation, the partial oxidation of proprene, and the partial hydrogenation of acetylene. The size dependence of the CO oxidation turn over frequency is shown in Fig. 16 which is the reaction rate per surface Au site per second. Clearly visible is the non-monotonous behavior as a function of the particle size. The turn over frequency is strongly peaked at about 3 nm which corresponds to ~ 300 atoms per cluster. It should be noted that these cluster are rather flat with a height of only about two to three atomic layers. Additional scanning tunneling microscopy/spectroscopy experiments showed that the catalytic activity is related to size effects with respect to the thickness of the gold islands with two-layer thick islands beeing most effective for the CO oxidation. At this cluster size also a band gap opens up with decreasing cluster size, i.e., a metal-to-nonmetal transition occurs [18]

Still the reasons for the large difference in the properties between bulk material and supported clusters is far from being fully understood. Several factors have been discussed so far that could be responsible for the difference: particle roughness, size dependence of the band gap, finite size effects or charge transfer phenomena.

Of course, these open questions have raised the interest of theoreticians in the properties of supported gold clus-

	E_b(eV)			
n	Au_n	Au_n^-	Au_n/Au(111)	Au_n/Au(111)$^-$
0	–	–	0.09	0.20
1	0.54	0.50	0.38	0.65
2	0.49	1.40	0.63	0.96
3	0.90	0.37	0.30	0.45
4	0.47	1.19	–	–
5	1.08	0.76	–	–

TABLE III: Binding energies of O_2 in eV on neutral and negatively charged Au(111), free Au_n clusters and supported Au_n/Au(111) clusters calculated by DFT calculations [144] ($n = 0$ corresponds to the flat Au(111) surface in the case of Au_n/Au(111)).

ters [143]. The theoretical treatment of nanosize particles by electronic structure theory methods still represents a great computational challenge. Due to the large number of symmetrically different atoms in nanostructures, the numerical effort required to treat these structures is enormous. On the other hand, there is definitely a need for the microscopic description of nanoparticles because the knowledge of the underlying mechanism leading to the modified nature of the particles is still rather limited. In this chapter, I will show the recent progress that has been made in the microscopic theoretical description of supported clusters. Usually the clusters treated in the theoretical studies are much smaller than the ones studied in experiments. Still some important qualitative aspects about cluster-adsorbate interaction can be learned from the theoretical studies as will be shown below.

In a fundamental study, Mills *et al.* studied the adsorption of O_2 on small free Au_n and supported Au_n/Au(111) clusters by DFT-GGA calculations [144]. They particularly focused on the role of the surface structure, the electron confinement, excess electrons and the band structure. The results of these calculations are summarized in table III. The calculations have been performed both for neutral as well as for negatively charged systems. The slab calculations for the supported clusters were performed within a 3×4 surface periodicity. The effect of the excess charges was also studied for the Au_n/Au(111) systems by adding one electron per unit cell which was then compensated by a homogeneous positive charge background. It should be noted that for the free Au_n clusters with $n \leq 3$ the calculations were checked by state-of-the-art quantum chemistry calculations [145], and significant differences were found which were attributed to the inaccurate description of oxygen in DFT. For the present discussion, however, these quantitative differences are not essentiell.

The adsorption geometries for O_2 on Au_5, Au/Au(111) and Au_3/Au(111) are shown in Fig. 17. All considered free Au_n clusters with $n \leq 6$ prefer a planar geometry, as for example the Au_5 cluster shown in Fig. 17a. In fact, there is no satisfactory explanation yet why these Au clusters are flat and do not condensate in a more compact structure. The O_2 bonding geometries on Au_n/Au(111) are in most cases similar to the corresponding bonding geometries on the free Au_n clusters which demonstrates that the O_2 adsorption is a rather local process. Indeed, an analysis of the electron density of the Au(111) slabs shows that the pertubation of the electronic structure due to the adsorption of O_2 is very efficiently screened by the metal electrons.

There is furthermore one common feature for all O_2 adsorption sites: O_2 does not bind on high-coordinated sites but rather at the edges of the clusters (see Fig. 17). At these edges, there are small regions with a high electron density. Such a configuration is favorable for electron transfer to the electronegative O_2 molecule which leads to bonding. On the other hand, on the flat Au(111) surface the electron distribution is rather smeared out without any regions of enhanced electron density. Consequently, the binding of O_2 on the flat Au(111) surface is very weak. However, there is also a complementary explanation in terms of the *d*-band model: low-coordinated sites have higher lying *d* states which interact more strongly with the adsorbate states [146]. Both views are appropriate and highlight different aspects of the bonding.

In addition, according to Table III O_2 binds stronger to the free Au_n cluster than to the corresponding supported Au_n/Au(111) with a single exception, neutral Au_2/Au(111). The supported clusters are strongly interacting with the underlying support. This removes electron density that could otherwise be used for binding O_2 at the low-coordinated sites of the clusters.

Nonetheless, low-coordination alone can sometimes not explain the reactivity. For example, at the Au_5 cluster the O_2 molecule does not bind to the two-fold coordinated corner atoms but rather to the two three-fold Au atoms in the upper part of Fig. 17a. This can be understood if the structure of the highest occupied molecular orbital of the cluster which interacts most strongly with the π^* orbital of O_2 is considered. Since Au_5 has an odd number of electrons, this orbital is in fact a singly occupied molecular orbital (SOMO [147]). The spatial distribution of this orbital is illustrated in Fig. 18. It is evident that the region in space where the SOMO of the *free* Au_5 cluster is mainly located coincides with the binding site of the oxygen molecule. At the two-fold coordinated corner atoms, there is only little weight of the SOMO.

However, it should be noted that these results for the O_2 adsorption on Au_5 are in conflict with the results of a similar study of oxygen molecular and dissociative adsorption on Au_n clusters [148]. In this study, the energetically most favorable O_2 molecular adsorption position on the Au_5 cluster was determined to be at the two-fold corner atoms. On the other hand, the important effect of the spatial distribution of the frontier orbitals for the energetically most favorable binding site has also been found in the adsorption of propene, C_3H_6, on small gold clusters and on Au(111) [147]. Thus the local electronic configuration at the low-coordinated sites has to be taken into account for a complete understanding of the binding

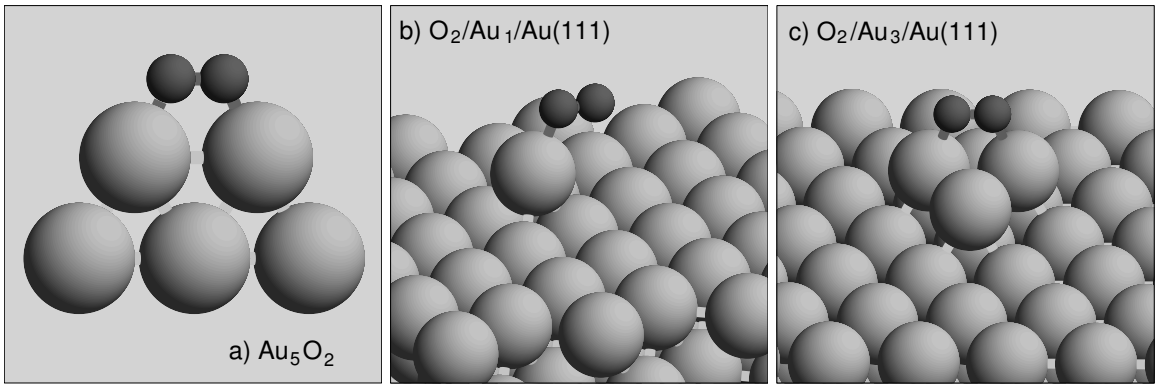

FIG. 17: Calculated optimal adsorption geometries of O_2 on Au_5, Au/Au(111) and Au_3/Au(111) (after [144]).

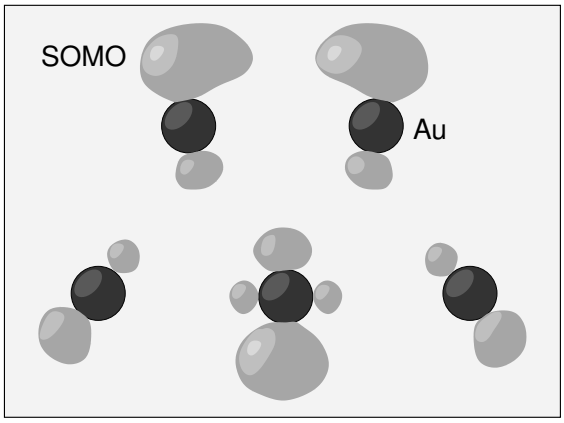

FIG. 18: Illustration of the spatial distribution of the singly occupied molecular orbital (SOMO) of Au_5 (after [144]).

properties.

The O_2 binding energy to the Au_n and Au_n^- gas-phase clusters is not correlated with the charge state of the clusters, but rather with the parity of the number of electrons. The valence electrons of a single Au atom have a $5d^{10}6s^1$ configuration, i.e. their number is odd. Au cluster with an odd number of electrons bind O_2 strongly; if there is an even number of electrons, O_2 is only weakly bound [149]. This means that paired electrons are apparently relatively inert, as far as the binding of O_2 is concerned. No such trend is obvious for the supported Au_n/Au(111) clusters, and the variation in the O_2 binding energies with the number n of atoms in the clusters is much less pronounced than for the free Au_n clusters.

There is, however, one clear trend: the O_2 binding energies to the Au_n/Au(111) clusters increases significantly when an extra electron is added to the unit cell. This additional electron ends up in the LUMO of the uncharged system which is localized at the site where the O_2 binds and thus contributes to the molecule-cluster interaction [144]. Thus both the low coordination as well the charging of the Au substrate lead to a strong O_2 binding.

The effect of the electron density in a nanostructure on the chemical reactivity was confirmed experimentally for a SnO_2 nanowire that was configured as a field-effect transitor [150]. By changing the electron density inside the nanowire through the applied gate voltage, the rate of oxygen adsorption and desorption and of CO_2 formation on the surface of the SnO_2 nanowire can be modified significantly.

The important role of the coordination of the Au atoms for the binding strength of oxygen has also been stressed by Nørskov and co-workers [146, 151, 152]. They calculated the adsorption energies of O and O_2 on a free Au_{10} cluster by DFT-GGA calculations and compared it to the corresponding adsorption energies on Au(211) and Au(111). (It should be noted that the adsorption energies of different groups differ due to technical details such as the exchange-correlation functional or the choice of the pseudopotential.) The Au_{10} cluster did not correspond to an energy minimum structure; rather a disklike geometry was chosen with seven atoms in the lower layer and three in the top layer (this structure is shown in Fig. 28) in order to mimic a Au cluster on a oxide support. On the cluster, the oxygen atom and molecule adsorb at the edges of the cluster. For example, the O_2 molecule binds to the lower plane in a geometry similar to the one shown in Fig. 17a. The O and O_2 binding energies are plotted as a function of the coordination number of the Au atoms in Fig. 19. It is obvious that there is a very strong dependence of the adsorption energies on the coordination number. Analogous trends have been also found in DFT calculations for CO adsorption on stepped Au surfaces and an Au adatom on Au(111) [153]. This confirms that low-coordinated atoms in nanostructures can act as preferential sites for atomic and molecular adsorption.

However, Fig. 19 also shows that the O_2 binding to Au(111) is stronger than to Au(211) although the coordination number of the Au atoms in the (111) surface is higher. Similarly, Liu *et al.* [154] have found that O atoms bind stronger to a Au(211) surface (coordination number 7) than to a kinked Au(211) surface (coordination number 6). For an oxygen atom on a Au adatom on Au(111) (Au/Au(111), coordination number 3), they even found that the atom is not stable with respect to the

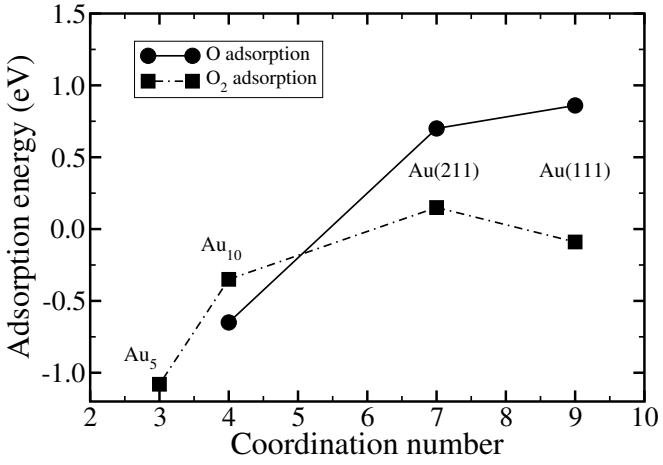

FIG. 19: Adsorption energies of O and O_2 on a Au_{10} cluster, on Au(211) and Au(111) plotted as a function of the coordination number of the Au atoms (after [146]). In addition, the results for the O_2/Au_5 and O_2/Au(111) by Mills *et al.* [144] are included. All the results have been obtained by DFT calculations using the PW91 functional [33].

associative desorption of O_2 into the gas phase which is surprising since the adsorbed O_2 molecule is stable (see Table III). Apparently, the coordination number is an important parameter in order to understand the interaction of atoms and molecules with specific sites, but there are other parameters such as the nature of the orbitals involved in the bonding [144] that are crucial for a complete understanding.

In order to make closer contact with the experiments of Au clusters supported by oxide substrates, the adhesion and shape of Au atoms and clusters on oxide surfaces has been addressed by several authors from a theoretical point of view [155–159]. These studies indicated the importance of defect sites for the adsorption of Au clusters. As far as single atoms are concerned, the binding of Au to an oxygen vacancy site on TiO_2 is substantially stronger than to the stoichiometric (110) rutile surface, as was found in a periodic DFT study [155].

Similar results were also found in DFT calculations for Au_n particles with $n = 1 - 3$ on the TiO_2 anatase (101) surface [156]. While the binding energies E_b of the Au_n particles on the stochiometric surface are typically between 0.3 eV and 0.8 eV (with the exception of Au_3 adsorbed in a bent geometry, $E_b = 1.9$ eV), the binding energies of these clusters on the reduced anatase surface with an oxygen vacancy are between 1.8 eV and 3.6 eV [156]. The strong binding is accompanied by a relatively large charge transfer to the gold atoms. Interestingly enough, CO interacts much more strongly with clusters adsorbed on the stochiometric surface than with clusters adsorbed on vacancies. This has been associated with the negative charge of the gold atoms which implies an unfavorable interaction with the dipole moment of the CO molecule [156]. However, it might also well be that the electrons involved in the strong bonding of the Au_n particles to the reduced surface are not available for the additional bonding of an adsorbate which then leads to the weak interaction.

It was furthermore found that the interaction between a monolayer of gold and a perfect rutile $TiO_2(110)$ surface is negligibly small [157]. On the other hand, if there are oxygen vacancies present, the interaction energy corresponds to -1.6 eV/defect. Thus it was concluded that the adhesion of gold to TiO_2 requires the presence of oxygen defects or possibly step and adatoms. The size and shape of supported particles can be derived from the Wulff construction [16] which is illustrated in Fig. 20: the particle is truncated in all directions at distances proportional to the interface or surface free energy of the crystal plane in that direction. This construction does not account for the formation energies for edge and corner atoms and is therefore only valid in the limit of large macroscopic crystals where the total formation energy of the edges is negligible compared to the total surface energies of the facets.

In order to account for defect and edge effects, Lopez *et al.* also included defect and edge energies estimated from calculations of slabs containing one to four gold layers [157]. Thus they found that Au particles with a diameter of 3-4 nm, such as the ones studied in the experiments [18] shown in Fig. 16, are three to four layers thick. This means that the Au particles are in fact rather flat, in good agreement with the experiment.

Already rather large Au nanoparticles on TiO_2 were addressed in DFT calculations by Molina *et al.* [159] using the RPBE functional. Since the nanosized Au clusters typically studied in the experiments are too large to be explicitly treated in DFT calculations, the authors chose just to model the interface between the nanoclusters and the substrate. They did so by replacing the nanoparticle with one-dimensional rods. One side of the rod was modeled according to the local bonding situation of the Au atoms at the edge of a nanoparticle while the other side of the rod only served the correct boundary conditions towards the interior of the supported clusters.

The general geometry of the one-dimensional rod model is illustrated in Fig. 21a, while Fig. 21b shows a side-view of the relaxed atomic structure of the Au rod on TiO_2 together with the optimal O_2 adsorption position. The adsorption studies are performed for $p(N \times 2), N = 2, 3$ surface unit cells using four trilayer TiO_2 slabs (in Fig. 21 only the two uppermost trilayers are shown). Four trilayers are necessary in order to account for the strong relaxation effects upon adsorption. The structure shown in Fig. 21 has been chosen to model a sharp Au particle termination. Another rod with a more rounded termination has also been considered in the study (see Fig. 22).

On clean, stochiometric $TiO_2(110)$, O_2 does not bind [161]. The interesting point is that the adsorption of O_2 on top of a Ti trough atoms (see Fig. 21) is strongly stabilized by the presence of a Au cluster with its edge above the adjacent bridging O atoms of the $TiO_2(110)$

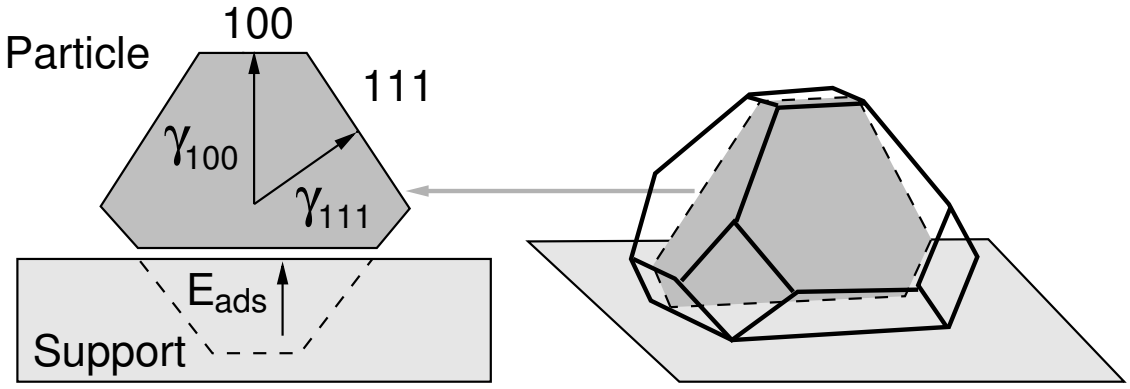

FIG. 20: Schematic illustration of a truncated Wulff polyhedron on a support. The left panel corresponds to a two-dimensional cut through the three-dimensional polyhedron in the right panel (after [158]).

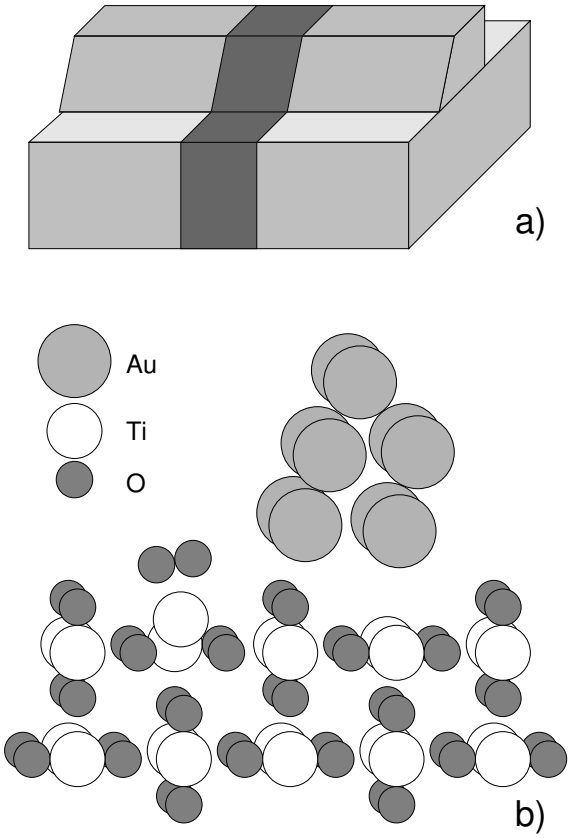

FIG. 21: Illustration of the one-dimensional rod model for the adsorption of O_2 an Au/TiO_2 nanoparticles used in GGA-DFT calculations. a) Schematic representation of the rod geometry. The dark-shaded area corresponds to the unit cell. b) Relaxed structure of O_2 binding at the Ti trough close to a supported one-dimensional Au rod with a sharp Au edge (after [159, 160]).

surface. An analysis of the charge density distribution shows that there is considerable charge transfer from the supported Au particle to the O_2 molecule mediated by the surface through electronic polarization. The O_2 molecule which is bound by 0.45 eV has a bond length of 1.41 Å indicating a charge state of the O_2 molecule close to the peroxo O_2^{-2} species. The O_2 adsorption is accompanied by a strong relaxation of the TiO_2 substrate with the Ti trough atom below the oxygen molecule pulled up by 0.8 Å. Furthermore, there is another weakly bound O_2 species (0.1 eV) within a leaning configuration connecting the Ti trough atom with the Au edge (see Fig. 22).

Since TiO_2 is a reducible oxide, a TiO_2 substrate with a bridging oxygen vacancy in the $p(3 \times 2)$ surface unit cell was also considered in the calculations. On the clean reduced TiO_2 surface, a O_2 molecule on the adjacent Ti trough atom becomes strongly bound by more than 1 eV. There is a significant charge transfer from the O vacancy to the O_2 molecule leading again to a peroxo O_2^{-2} species. The O_2 binding energy is even further increased to 1.65 eV if the edge of the Au rod is located above the O vacancy. This suggests that the Au rod provides additional charge for the binding of the O_2 molecule. The Au rod does in fact only weakly interact with the O vacancy so that the adsorption configuration is very similar to the one for the stochiometric TiO_2 surface. This is different if a single Au atom is located at the vacancy site. Then the O_2 binding energy is reduced to 0.64 eV because of the competition between the O_2 molecule and the low-coordinated, reactive Au atom for the electrons of the vacancy [159].

As far as the CO oxidation is concerned, it turned out that the Au rod with the sharp edge binds CO very weakly. This is caused by the unfavorable orientation of the CO molecule with respect to the edge because of the presence of the substrate. On the other hand, at the Au rod with the rounded edge the CO molecule can bind rather strongly ($\sim$ 0.5 eV) to the low-coordinated Au atoms of the second layer, as illustrated in Fig. 22. This binding is only weakly influenced by the presence of O_2 on the substrate.

The structure shown in Fig. 22 with a leaning O_2 molecule and the CO bound to the second layer of the Au rod represents a favorable initial configuration for the CO oxidation because of the small binding energy

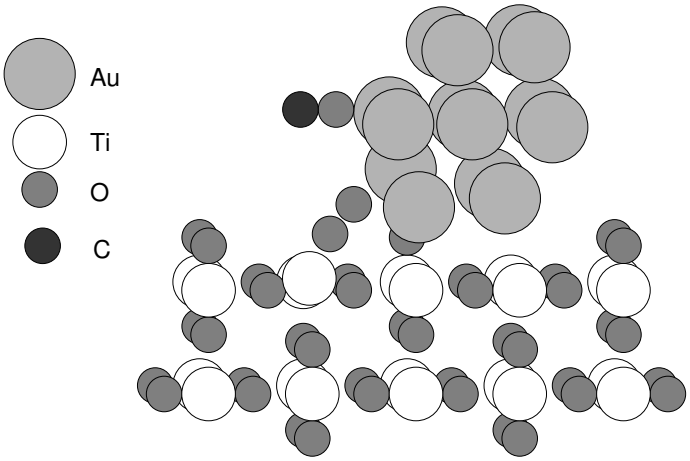

FIG. 22: Minimum energy structure of a leaning O_2 molecule and a CO molecule bound to a Au rod on TiO_2 with rounded shape and the oxygen vacancy situated below the nanoparticle edge (after [159]).

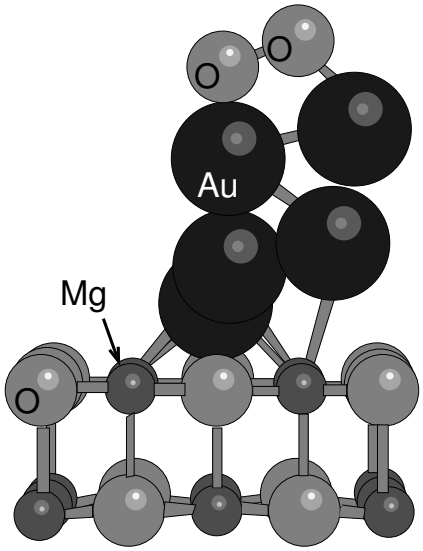

FIG. 23: Most favorable O_2 adsorption site on an Au_8 cluster adsorbed on a MgO(100) surface containing an oxygen-vacancy F-center. Due to the perspective, not all Au atoms are visible (after [8])

of the O_2 molecule. The O_2 molecule can approach the CO molecule and react with the CO to CO_2 rather easily. The CO_2 formation according to a Langmuir-Hinshelwood mechanism is only hindered by a barrier of 0.15 eV with the remaining O atom bound on top of a Ti trough atom.

However, the fact that oxygen vacancies are required for the adhesion of gold on titania seems to be at variance with recent experimental findings that gold monolayers and bilayers can completely wet, i.e. cover the titania support [162]. In this particular study, it was also found that the gold bilayer structure is significantly more active with respect to CO oxidation than the monolayer structure. This also means that the O_2 molecule involved in the CO_2 formation cannot bind to the TiO_2 substrate. In spite of the detailed investigations already performed for the Au/TiO_2 system, certainly further experimental and theoretical studies are needed to fully understand the exceptional activity of Au nanostructures supported on oxide substrates.

On the other hand, the important role of oxide defects for the catalytic activity of supported Au particles was verified both in experiment as well as in theory [8] for another oxide support material, namely MgO(100). In a combined experimental and theoretical study, the CO oxidation catalyzed by size-selected Au_n clusters with $n \leq 20$ supported on defect-poor and defect rich MgO(100) films was investigated [8]. These experiments are different from the ones reported for Au/TiO_2 insofar as, first, the clusters used are much smaller, and second, the cluster were size-selected before deposition so that a monodispers distribution of Au clusters was deposited on MgO(100). The experiments revealed that the gold clusters deposited on defect-rich MgO-films have a dramatically increased activity compared to clusters deposited on defect-poor films at temperature between 200 and 350 K. The smallest catalytically active particle was found to be the Au_8 cluster.

In order to detect the microscopic mechanisms underlying the observed behavior, LDA-DFT calculations have been performed describing the oxide substrate in a finite setup [8]. Between 27 and 107 substrate atoms have been embedded into a lattice of about $2000 \pm 2\,e$ point charges at the positions of the MgO lattice. As a defect, an oxygen-vacancy F-center was introduced at the MgO(100) surface. The equilbrium shape of a Au_8 cluster adsorbed on the defect-free MgO surface and on the F-center was determined, and the energetically most favorable adsorption sites for O_2 and CO and the reaction paths of the CO oxidation catalyzed by the Au_8 cluster were explored. A side view of the Au_8 cluster located above the F-center is shown in Fig. 23. The structure of the Au_8 cluster corresponds to a deformed close-packed stacking.

In addition, in Fig. 23 the energetically most favorable adsorption position of O_2 on the Au_8 cluster is illustrated. This position corresponds to an edge-top configuration on the triangular top-facet of the Au_8 cluster. At this site, the O_2 adsorption energy is $E_a = 1.22$ eV which is rather large compared to the values for the free Au_n and the supported $Au_n/Au(111)$ clusters (see Table III, however, the adsorption energy might well be overestimated because of the notorious overbinding occuring in LDA calculations [16]). This high adsorption energy is believed to be caused by the partial electron transfer of $0.5\,e$ from the MgO(100) surface to the gold octamer, according to the analysis of the electronic structure of the cluster [8]. On a Au_8 cluster supported on the stochiometric MgO(100) surface, the O_2 binding energy is much lower, only about 0.5 eV[163]. O_2 can also adsorb

at other sites on the Au_8 cluster, for example in an edge configuration of the top-facet (E_a = 0.88 eV) or even at the interface of the Au_8 cluster periphery with the MgO substrate. At all these adsorption sites, the oxygen molecule is found to be in a peroxo, i.e. O_2^{2-} state with a weakened highly stretched intramolecular bond (d_{O-O} = 1.41 − 1.46 Å) compared to that of the free molecule (d_{O-O} = 1.24 Å).

Another important aspect for the reactivity of small supported clusters is their dynamic structural fluxionality [163]. They are able to adapt their structure in order to provide energetically favorable adsorption sites. For the Au_8 cluster supported on the stochiometric MgO(100) surface, it was indeed found that constraining the cluster to its original geometry prevents the adsorption and activation of O_2 [163].

The adsorption configuration shown in Fig. 23 acts as a favorable initial configuration for the CO oxidation. A CO molecule approaching this adsorbed O_2 molecule can react spontaneously with the oxygen molecule to form a weakly bound (~ 0.2 eV) CO_2 molecule that can directly desorb plus an adsorbed oxygen atom. Such a mechanism is called an abstraction or so-called *Eley–Rideal mechanism*. Recall that although the CO oxidation is strongly exothermic, it is hindered by a large activation barrier in the gas phase. Another reaction pathway that has been found is of the Langmuir-Hinshelwood type which means that the two reactants are initially coadsorbed on the top-facet of the Au_8 cluster. This CO oxidation path has a similarly small barrier. Through these reaction channels the low-temperature CO oxidation down to 90 K can proceed. As far as the higher-temperature oxidation is concerned, further channels have been identified at the periphery of the gold cluster. Their barriers are much smaller at the Au_8 cluster adsorbed above the F-center than on the perfect surface giving an explanation for the enhanced activity of the clusters on the defect-rich substrate. A similar effect has been found in a combined experimental and theoretical study addressing the reactivity of nano-assembled Pd catalysts on MgO thin films [164] where, however, the Pd catalysts were just modeled by single atoms in the calculations.

The CO oxidation at MgO supported gold aggregates was also addressed in a DFT study by Molina and Hammer [158, 160] who particularly focused on the role of the oxide support for the CO oxidation. As a first step, the shape of adsorbed gold particles was determined using the Wulff construction which is illustrated for a two-dimensional cut in the left panel of Fig. 20. According to the calculated surface energies of Au low-index faces and the Au-MgO adhesion energies, the Au clusters assume a partial wetting shape as shown in the right panel of Fig. 20, in agreement with the experiment [165].

However, as already mentioned above, the Wulff construction does not account for the formation energies for edge and corner atoms and is therefore only valid in the limit of macroscopic crystals where the edge and corner energies do not play any role. For smaller clusters, the assumption of negligible total edge and corner energies is no longer justified. And indeed, Molina and Hammer found that the energetically most stable structure of a Au_{34} cluster on MgO does not look like the one shown in Fig. 20. The supported Au_{34} cluster rather shows a increasing degree of partial wetting, i.e., the cluster assumes a flat shape with a enlarged interface area between support and cluster.

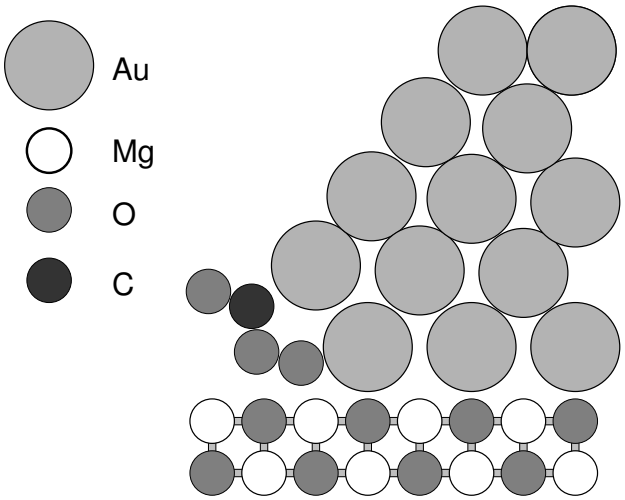

FIG. 24: Schematic drawing of the CO · O_2 binding configuration at an Au-MgO interfacial structure modeled by an one-dimensional rod structure in GGA-DFT calculations (after [158]).

In a second step, the adsorption of CO, O_2 and the CO oxidation at the MgO supported gold aggregates were studied. Again, like in the study by Molina *et al.* of TiO_2 supported Au nanoparticles [159], the nanoparticles where replaced by an one-dimensional rod within a MgO(100)-(5×2) geometry. One of the considered rod structures is depicted in Fig. 24. CO and O_2 are found to adsorb on these rods at low-coordinates sites in the "equatorial plane". The O_2 binding energies, however, are much smaller (∼0.2 eV using the PW91-functional) than on the small Au_n clusters with $n \leq 10$ [144, 146]. The O-O bond length is extended from the gas phase value of 1.24 Å to 1.35 Å corresponding to a superoxo O_2^- species. Atomic oxygen binds to the low-coordinated sites of the Au rods with adsorption energies that are much larger than on the flat Au(111) and Au(100) surfaces. Furthermore, the O_2 dissociation barriers are rather large (∼1 eV) so that they were excluded as possible routes in the low-temperature CO oxidation. Instead, relatively stable peroxolike $CO{\cdot}O_2$ reaction intermediates with total binding energies of about 1 eV were identified in the DFT calculations. The most stable of the $CO{\cdot}O_2$ complexes is shown in Fig. 24.

This complex is in fact more stable by about 0.1 eV than the separate adsorption of CO and O_2. In order to understand this stabilization, the substrate-induced charge redistribution has been analysed in detail. As

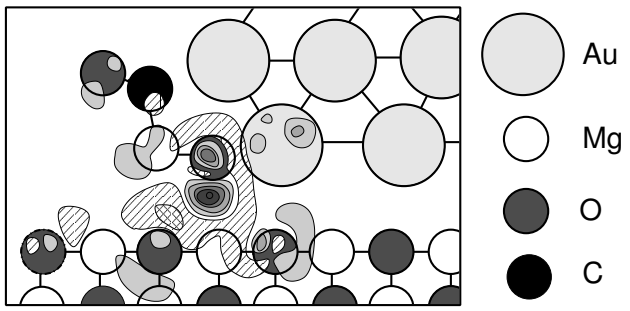

FIG. 25: Charge density difference plot of the MgO-induced charge redistribution derived from DFT calculations. Shaded areas correspond to charge accumulation while hatched areas denote charge depletion (after [159]).

Fig. 25 shows, there is an induced charge accumulation between a Mg atom and the terminal peroxo oxygen atom while there is charge depletion at the oxide. Thus the stabilization is mediated by a charge transfer which leads to an additional attractive interaction. The energy barriers associated with the CO_2 formation from the $CO{\cdot}O_2$ complexes are rather low ($\sim$ 0.3 eV) which means that the CO oxidation can readily occur already at room temperature which is in agreement with experiments for the Au/MgO system [166].

This shows that the MgO support plays an active role in the bonding and activation of adsorbates bound to supported gold particles. However, it should be emphasized that this role is much less dramatic than for TiO_2 [159] where the reduced substrate not only provides charge for the binding of the O_2 molecule but actually binds the O_2 molecule.

As already discussed in the previous section, the promoting or poisoning effect of coadsorbates is an important issue in heterogeneous catalysis. The most well-known example for poisoning is the reduction of the activity of the platinum-based car-exhaust catalyst by lead present in the gasoline. Two studies have addressed the influence of coadsorbates on the catalytic performance of the MgO-supported Au nanoparticles. Häkkinen *et al.* considered the Au_n cluster shown in Fig. 23 to which the electron donor strontium was added [163]. This choice was motivated by the fact that the electron transfer to the Au_8 cluster seemed to be crucial for the understanding of the enhanced catalytic activity of the nanoparticle. And indeed, experiments revealed that pure MgO-supported Au_n clusters with $n \leq 7$ are catalytically inert as far the CO_2 production rate per deposited cluster is concerned, whereas supported Au_nSr clusters are catalytically active already for $n \geq 3$.

DFT calculations have confirmed the enhanced adsorption and activation of O_2 on the Sr-doped systems. Exchanging one Au atom by Sr of a MgO-supported Au_4 cluster modifies the adsorption properties significantly.

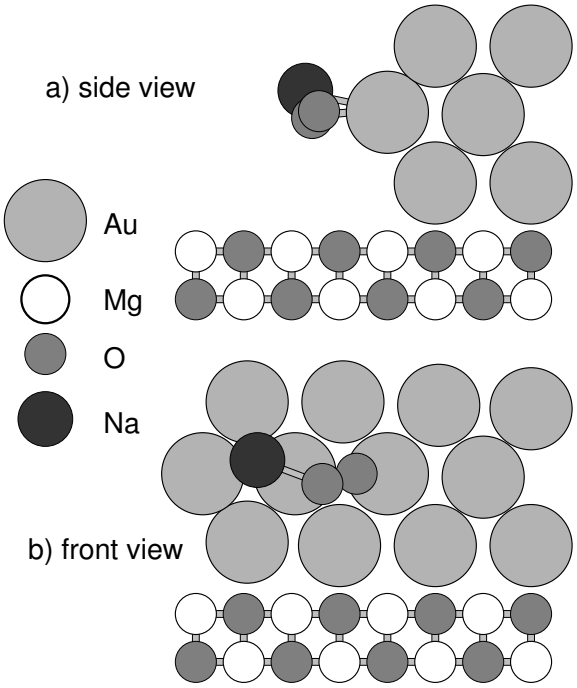

FIG. 26: Side and front view of the stable adsorption configuration of O_2 at a Na-decorated edge of a Au rod deposited on MgO according to DFT-GGA calculations (after [167]).

The oxygen molecule bonds mainly to the strontium atom of the Au_3Sr cluster with a considerably higher adsorption energy of 1.94 eV compared to 0.18 eV on the supported Au_4 cluster. The stronger interaction is caused by additional electron transfer to the O_2 molecules made possible by the charge provided by the Sr atom. This results in a superoxo-like state of the adsorbate which is reflected in an increased O-O bond length of 1.37 Å [163].

The coadsorption of both a single electron donor (Na) and a single electron acceptor (Cl) were considered in a *ab initio* study by Broqvist *et al.* [167] using the approach illustrated in Fig. 24 to replace the supported nanoparticle by an one-dimensional rod. In the coadsorption study, however, a smaller rod was used consisting only of the first three Au layers as shown in Fig. 26. The most favorable adsorption positions for both Na and Cl are at Au bridge sites of the second layer, i.e., at the Au layer sticking out into the vacuum. As expected, Na adsorbs as a positively charge ion and Cl as a negatively charged ion, i.e. there is significant charge transfer to and from the Au rod, respectively. However, the Na adsorption position is only metastable with respect to exchanging its position with a Au atom. Although Na prefers the low-coordinated site *in adsorption*, it rather absorbs into the Au rod forming a NaAu alloy.

The effects of the Na and Cl adsorption on the interaction of the rods with O_2, O, CO and the $CO{\cdot}O_2$ complex are summarized in table IV. At the Na-decorated Au edge, the O_2 binding is increased by 0.2 eV with respect to the clean Au edge. This increase is caused by the for-

	E_b(eV)		
	Au/MgO	Na/MgO/Au	Cl/Au/MgO
O_2	0.13	0.33	-0.20
O	0.13	0.84	0.03
O	0.75	0.52	0.60
$CO{\cdot}O_2$	0.98	1.62	0.49

TABLE IV: Calculated binding energies of O_2, O, CO and the $CO{\cdot}O_2$ complex in eV on Au/MgO models with a clean, a Na-decorated and a Cl-decorated Au edge [167], respectively. A negative binding energy corresponds to unstable adsorption.

mation of a chemical bond between Na and O together with the higher capability of the Au rod to donate electrons to oxygen because of the additional electron provided by the Na atom. This stable adsorption configuration is illustrated in Fig. 26. Also the adsorption energy of atomic oxygen is strongly enhanced. Interestingly, CO binds less strongly to the Na-decorated edge, its binding energy is reduced by 0.2 eV compared to the undecorated Au edge. It was suggested that the reduced binding is a consequence of the Na-induced down-shift of 0.09 eV of the local *d*-band center at the Au edge [167]. However, this downshift seems to be too small to explain such a large reduction in the CO binding energy.

On the other hand, the adsorption of the $CO{\cdot}O_2$ complex shown in Fig. 24 is again strongly promoted by the presence of Na atoms at the Au edge. The binding energy of the $CO{\cdot}O_2$ complex at the Na-decorated edge is 1.6 eV which is almost twice its binding energy at the clean Au edge. The reason for this increased stability is again the formation of a Na-O_2 bond. Hence Na acts as a promoter on the Au nanoparticles but its promotive character is related to the formation of strong Na-O bonds.

In contrast to Na, Cl has a poisoning effect when it is adsorbed at the Au edge. Its presence makes the O_2 adsorption unstable and reduces the O and CO binding energy. Furthermore, it makes the $CO{\cdot}O_2$ complex less stable by 0.5 eV. The poisoning effect of Cl is caused by an electrostatic repulsive interaction with the negatively charged adsorbates. Even for larger distances between the Cl atoms and the adsorbates, this repulsive interaction is still present due to the long-range character of the Coulomb interaction. The promoting effect of Na, on the other hand, is short-ranged because of the local nature of the attractive Na-O bonds.

Not only Au clusters deposited on MgO have been considered in *ab initio* electronic structure calculations. The adsorption properties of Ni_4 and Ni_8 clusters supported on regular and defect sites of the MgO(001) surface were studied in a DFT study, in which the oxide substrate was modeled by a $Mg_{13}O_{13}$ cluster embedded in two layers of 16×16 point charges each (PC=2e) in order to reproduce the correct Madelung potential at the adsorption site under study [168]. The structure of the supported Ni_4 and Ni_8 cluster was optimized under the constraint of the

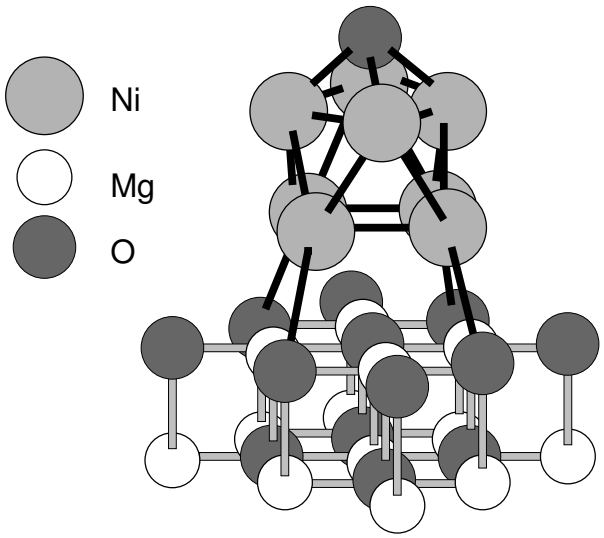

FIG. 27: Optimized structure of an oxygen atom adsorbed on a Ni_8 cluster supported on Mgo(001). The oxide substrate is modeled by a $Mg_{13}O_{13}$ cluster embedded in two layers of 16×16 point charges each (PC=2e) [168].

C_{4v} symmetry, i.e., a fourfold symmetry was deliberately imposed on the clusters. Thus the cluster do not necessarily correspond to minimum energy structures. The study was not meant to give quantitative results, but rather qualitative trends with respect to the size and the MgO adsorption site of the supported cluster.

Atomic oxygen and sodium have been used as adsorbates in the calculations to probe the reactivity of the clusters. The optimized structure of atomic oxygen on the supported Ni_8 cluster is shown in Fig. 27. It is obvious that the Ni_8 cluster is much less distorted than the Au_8 cluster on MgO(001) (see Fig. 23), probably because of the symmetry constraints used in this Ni/MgO study. The optimized structure of the supported Ni_4 cluster corresponds basically to the first layer of the Ni_8 cluster. The Ni cluster were also positioned above a neutral and positive oxygen vacancy, a F_s or F_s^+ center respectively. Furthermore, the oxygen and sodium adsorption energies were also determined for free, unsupported Ni clusters.

First of all, the DFT calculations have confirmed that the metal clusters are much more strongly bound to the oxygen vacancy sites than to the stochiometric MgO surface [169]. Almost indepedent of the charge state, the binding energies are enhanced by more than 1.5 eV. The larger cluster interacts more strongly with all considered MgO surfaces which can be explained by its higher polarizability [168].

For atomic oxygen, the adorption energies on the supported clusters are in fact larger than on the free Ni cluster. The interaction of the electronegative oxygen with metal surfaces and clusters is characterized by a significant charge transfer to the oxygen atom. For the supported cluster, the oxygen anions of the surface act as an additional source of electrons increasing the charge

transfer to the oxygen atom and thus its binding energy. For the cluster above the oxygen vacancies, the binding is further enhanced since the F centers represent an additional source of charge transfer. In the case of the F_s^+ center, there is also the electrostatic attraction between the negatively charged adsorbed oxygen atom and the positively charged vacancy.

The effect of the vacancies on the atomic oxygen adsorption energies is particularly pronounced for the planar Ni_4 cluster where is leads to an increase of about 1 eV. For the three-dimensional Ni_8 cluster, however, the atomic oxygen adsorption energies are basically independent of the presence or absence of defects in the MgO substrate. This indicates that for the Ni/MgO system the influence of the vacancies on the electronic structure of the supported clusters is restricted to the first layer, obviously in contrast to the Au/MgO system [8].

The electropositive sodium atom binds much weaker to the Ni clusters than the more electronegative oxygen atom. On the Ni clusters deposited on both the stochiometric MgO surface and the positively charged oxygen vacancy, sodium adsorbs as an anion, as an analysis of the dipole moment as a function of the vertical displacement shows [168]. Above the neutral oxygen vacancy, however, sodium is only partially charged since the electrons donated from the vacancy to the Ni cluster prohibit the charge transfer from the sodium to the metal atoms. In spite of these different bonding characteristic, the Na bonding energies are only very weakly dependent on the cluster size and MgO adsorption site which is rather surprising. It has been speculated that this might be due to the cancellation of opposing effects [168].

So far we have shown that the high density of low-coordinated sites at oxide-supported metal nanoparticle leads to a stronger interaction with adsorbates. Even the oxide support can act as a promoter for the bonding and activation of adsorbates on the metal particles. However, there is another effect which can counterbalance the promoting effect of the low coordination of the nanoparticles, namely the interatomic relaxation of the small particles. This leads to reduced interatomic distances which, together with a strong cluster-support interaction, can cause a weaker interaction with adsorbates.

The important influence of the interatomic distances on the adsorption properties has been found in DFT calculations for small Pd_n cluster (n = 3,7,10) on Au(111) [170]. Transition metal cluster supported on inert noble metals are of particular interest in the field of electrochemistry [171] because the substrate has to be conductive so that supported nanostructures can act as electrodes. Furthermore, the electrochemical STM can be used for the nanostructuring of electrode surfaces. Based on the *jump-to-contact* between STM tip and sample, highly ordered arrays of metal clusters containing of the order of only one hundred atoms can be generated [171–173]. These nanofabricated clusters exhibit an unusual electrochemical stability. It has been speculated that this stability might be caused by quantum size effects in the metal particles [171]. Furthermore, it has been shown that the catalytic activity of Pd clusters supported on a gold surface towards electrochemical hydrogen evolution is enhanced by more than two orders of magnitude when the diameter of the palladium particles parallel to the support surface is decreased from 200 to 6 nm [174, 175].

In order to understand the chemical properties of the Pd/Au particles, in a first step the binding energies of hydrogen and CO on pseudomorphic Pd/Au overlayers has been evaluated by DFT calculations [54, 55]. These calculations have demonstrated that both the expansion of the pseudomorphic overlayers by 5% as well as the relative weak interaction of the Pd overlayer with the gold substrate lead to a stronger interaction with the adsorbates compared to a bulk Pd substrate. Both effects which can again be understood within the *d* band model enhance the adsorption energies on Pd/Au(111) by a similar amount which is about 0.10-0.15 eV.

The adsorption energies of CO located at different sites of Pd_{10} clusters supported by Au(111) are shown in Fig. 28. Interestingly enough, all the CO binding energies are lower than those on pseudomorphic Pd/Au(111) overlayers. This means that for this system CO binds less strongly to low-coordinated cluster atoms than to high-coordinated atoms in pseudomorphic overlayers. The same results have also been found for atomic hydrogen adsorption energies.

In order to understand these results, it is important to analyse the nearest-neighbor Pd-Pd distances. The calculated value for Pd bulk is 2.80 Å, for Au bulk 2.95 Å. This means that the pseudomorphic Pd films on Au are expanded by 5%. Fig. 28 also shows the Pd-Pd nearest-neighbor distances of the supported Pd_n clusters. Although these clusters are supported by a gold substrate, their nearest-neighbor distances of 2.76 Å are even below the Pd bulk value. These reduced distances are a consequence of the low coordination of the cluster atoms which makes the single Pd-Pd bonds stronger than in a bulk situation where every Pd atom is twelve-fold coordinated. At the second layer of the Pd_{10} cluster, the Pd-Pd distances are even further reduced to 2.65 Å. Note that for the free relaxed planar Pd_3 and Pd_7 cluster, the nearest neighbor distances are 2.50 Å and 2.64 Å, respectively.

The reduction in the interatomic distances results in a larger overlap of the *d* orbitals which leads to a broader local *d*-band and a down-shift of the local *d*-band center because of charge conservation, as confirmed by the DFT calculations for the Pd_{10} clusters supported on Au(111) [170]. This is the opposite process of the one illustrated in Fig. 3 where a smaller overlap between the *d*-band metal atoms had been considered. Thus the reduced binding energies on the Pd atoms can be understood within the *d*-band model.

In Fig. 28, the CO adsorption energies on free Pd_{10} clusters in exactly the same configuration as the supported clusters are also given by the numbers in parentheses. These binding energies are in fact larger than on

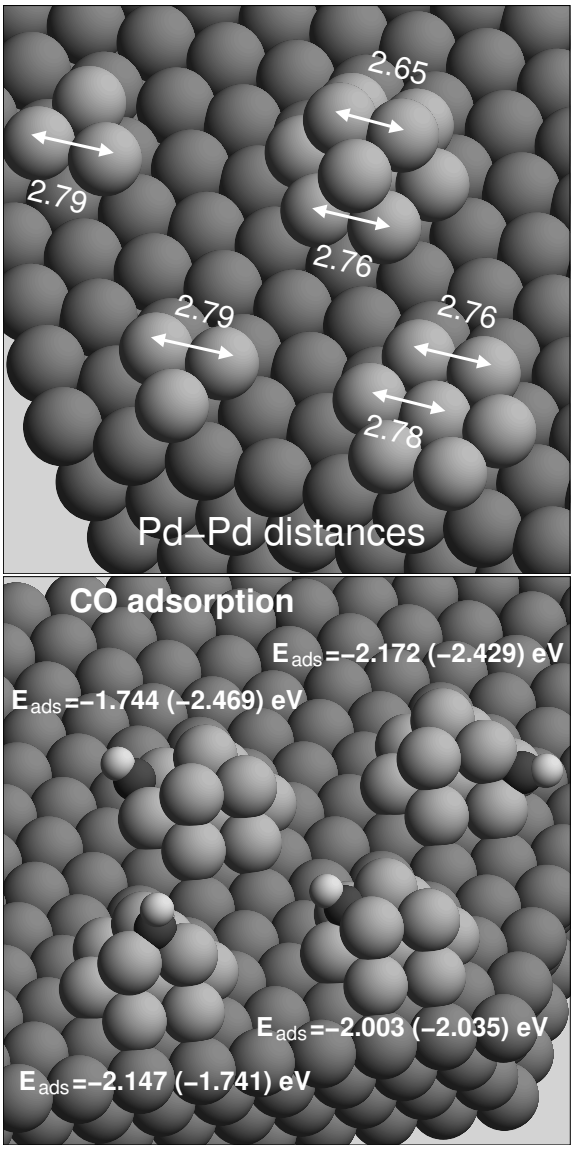

FIG. 28: Calculated nearest-neighbor Pd-Pd distances in Å of Pd_n cluster supported by Au(111) and CO adsorption positions and energies on the Pd_{10}/Au(111) cluster. The energies in parentheses correspond to the adsorption energies on free Pd_{10} clusters in exactly the same configuration as the supported clusters (after [170]).

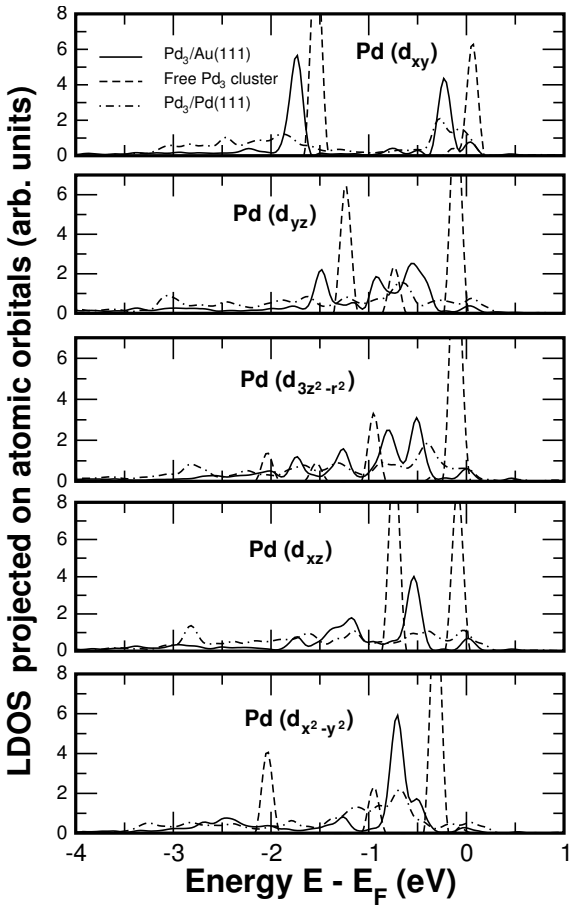

FIG. 29: Orbital resolved d-band local density of states (LDOS) of the supported Pd_3/Au(111) and Pd_3/Pd(111) clusters and the free Pd_3 clusters determined by DFT calculations (after [170]).

the supported clusters and also on flat [86] and stepped Pd surfaces [89]. This shows that in spite of their compression free clusters can still be much more reactive than surfaces because of their low coordination. Thus it is the interaction of the Pd clusters with the Au support that contributes to the low binding energies on the metal-supported clusters.

Interestingly enough, at the top layer adsorption site of the Pd_{10} cluster, the CO binding energies on the free cluster are smaller than on the supported cluster. This surprising result is caused by the reactivity of the unsaturated hexagonal bottom layer of the free Pd_{10} cluster. It binds the three topmost Pd atoms so strongly that the top layer becomes less reactive, as an analysis of the energetics and the electronic structure of the free cluster confirms [170].

The coupling of the Pd clusters to the underlying Au substrate can also be revealed by analysing the electronic structure of the system. In Fig. 29, the orbital resolved d-band local density of states (LDOS) for Pd_3 clusters deposited on Au(111) and on Pd(111) and for a free Pd_3 cluster is plotted. The free cluster exhibits a discrete structure of electronic levels, as is expected for a finite system. As far as the Pd_3 cluster supported on Au is concerned, all d-band orbitals that are confined within the cluster layer, i.e. the d_{xy} and the $d_{x^2-y^2}$ orbitals, also show a rather discrete structure. This means that these orbitals are localised within the cluster. The LDOS of the other three orbitals that have a component along the vertical z-direction is rather broad. This indicates that these states are already delocalized because of their significant coupling to the electronic states of the Au support. For the Pd_3/Pd(111), *all* d states in the cluster are considerably broadened (see Fig. 29) demonstrating an

even stronger coupling between the cluster and the substrate.

As alredy mentioned, it has been speculated that the unusual electrochemical stabibility of nanofabricated supported metal clusters [172] could be caused by quantum confinement effects [176] that would lead to a discrete electronic spectrum in the clusters. However, the DFT calculations yield a continuous spectrum already for small supported Pd_3 clusters. For larger clusters, any quantum confinement effects would even be smaller. Thus these calculations do not support the speculation of Ref. [176].

As an alternative explanation it has been proposed [177, 178] that the electrochemical nanofabrication of the clusters by the jump-to-contact leads to an alloying of the clusters which causes their high electrochemical stability. The deposition of the clusters has been simulated using classical molecular dynamics with the interatomic interaction described within the empirical embedded-atom-method (EAM) [179, 180]. The stability of the deposited clusters was then analysed by grand-canonical Monte Carlo simulations which took the electrochemical potential into account [181]. The simulations indicate that electrochemically stable clusters occur only in those cases where the two metals that are involved form stable alloys. In fact, DFT calculations also indicate that the Pd_{10} clusters on Au(111) [170] are stabilized by 0.1 eV if one of the Pd atoms at the base of the cluster is exchanged with an Au atom of the underlying substrate [182].

The possibility of intermixing or alloying is always an important issue in the case of bimetallic systems [183]. Recently, the electronic and chemical properties of Mo nanoparticles on Au(111) were studied experimentally [184]. This study was motivated by the fact that the nanoparticles can act as precursors for the preparation of molybdenum sulfide and molybdenum oxide aggregates [185, 186] which are widely used catalyst materials in the chemical industry [114]. The Mo particles were deposited by dosing $Mo(CO)_6$ at temperatures high enough so that $Mo(CO)_6$ decomposes thus creating Mo on the surfaces. DFT calculations of the $Mo(CO)_6$ defragmentation process indicate that the decomposition is an activated process which might be facilitated by the presence of defects on the surface [187].

Furthermore, the experiments indicated that CO does not adsorb on the Mo/Au(111) surface [184]. However, the exact structure of the Mo nanoparticles on Au(111) could not be determined experimentally. Therefore, DFT calculations were performed in order to study the structure and chemical properties of Mo nanoparticles on Au(111) [188]. Several structural models of the Mo/Au(111) system were investigated within a (2×2) surface unit cell. Two of them are shown in Fig. 30. The difference between the two structures is that the open Mo structure in Fig. 30a has been filled up with Au atoms in Fig. 30b yielding a flat (111) surface.

The stability of the surface structures has been determined with respect to bulk Au and bulk Mo, i.e. it was assumed that the formation energy of both bulk Au and bulk Mo is equal to zero. It turns out that Mo actually prefers to be embedded in the gold surface [187, 188]. The structure shown in Fig. 30b is by 0.3 eV/atom more stable than the one of Fig. 30a. One gains even another 0.01 eV/atom if the surface is fully covered by Au atom, i.e. if a Au-Mo-Au sandwich structure is formed.

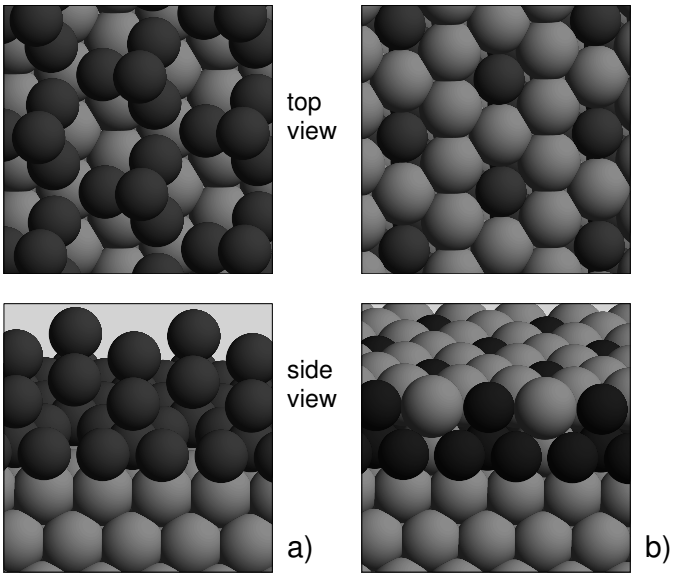

FIG. 30: Top and side view of two Mo/Au(111) structures studied by DFT calculations [188]. The light and dark balls represent Au an Mo, respectively..

In order to analyse the reactivity of the Mo/Au(111) surface structures, the adsorption of CO, oxygen and sulfur has been used as a probe. The adsorption of CO on both structures shown in Fig. 30 is exothermic, the CO binding energies are 2.22 eV and 1.03 eV for the structures a and b, respectively, using the RPBE functional. Interestingly enough, the binding energy of CO on one Mo monolayer on Au(111) is even larger, 2.79 eV. In this respect the Mo/Au system behaves like the Pd/Au system [170]: The nearest-neighbor distances in Mo are 5% smaller than in Au so that the pseudomorphic Mo overlayer on Au is significantly expanded. This results in a significant upshift of the d-band center and consequently in stronger interaction energies with adsorbates.

The experimental findings that CO interacts very weakly with the Mo/Au(111) system can only be reconciled with the experimental results by assuming that they are caused by Mo-Au site exchange and Au segregation to the surface. This means that Mo nanostructures on Au are not stable, so that this system does also not exhibit any special chemical properties related to the limited size of the Mo particles, but rather behaves like a pure Au(111) surface.

In the case of the adsorption of oxygen and sulfur on the Mo/Au(111) system, the same qualitative trends have been found as for CO adsorption. Furthermore, two

other admetals, Ni and Ru, were considered in the DFT calculations [188] in order to check whether they show a similar behavior as Mo on Au(111). And indeed, Ni and Ru also tend to mix with a Au substrate. In addition, the qualititative trends in the adsorption properties of the systems Ni/Au(111) and the Ru/Au(111) resemble the ones found in the Mo/Au(111) system. Thus once the metal nanoparticles are embedded in the Au matrix, these bimetallic systems only exhibit properties of gold.

V. NANOSTRUCTURING OF SURFACES BY ORGANIC TEMPLATES

So far we have only dealt with atomic and molecular adsorption *on* nanostructured surfaces. However, ordered arrays of adsorbed molecules can in fact lead to a nanostructuring of otherwise flat surfaces. In particular *organic* adsorbates can induce a nano-patterning in the form of ordered overlayers or molecular wires. This phenomenon is often also discussed in the context of self-organization and self-assembly on surfaces [189]. It has been suggested that the spontaneous self-assembly of DNA-base molecules on mineral template surfaces may play an essential role for the origin of life under prebiotic conditions [190, 191]. These layers could act as a template for the assembly of higher ordered polymers. Furthermore, these structure might also be technologically relevant in the context of sensing, catalysis, or molecular electronics. These aspects have therefore motivated STM studies of DNA-bases self-assemblied as two-dimensional crystalline films [192, 193].

As a substrate for organic overlayers, often highly ordered pyrolytic graphite (HOPG) [192–194] or noble metals substrates [122, 195, 196] are used since these substrates are relatively inert so that the organic molecules are not significantly perturbed by the presence of the surface. The substrate might just serve as a template to fix the molecules in space, but in general the resulting self-assemblied supramolecular structures are a consequence of a subtle balance between molecule-molecule and molecule-substrate interactions. Only in the case of a sufficiently strong adsorbate-surface interaction, surface rearrangement induced by the adsorption might occur.

Several experimental studies addressing self-assemblied organic overlayers have focused on the purine base adenine (6-aminopurine, C_5,H_5N_5) whose molecular structure is shown in Fig. 31. Yet, STM and atomic force microscopy (AFM) experiments of adenine adsorbed on graphite did not yield any atomic resolution [192, 197]. In the STM images, some ordered structure is visible, however, no microscopic adsorption configuration can be deduced. Combining the information from the STM with reciprocal space data from low-energy electron diffraction (LEED) experiments, a unit cell of rectangular shape with dimension 22 Å×8.5 Å was proposed [198]. Although also the symmetry of the molecular structure within the surface unit cell could be

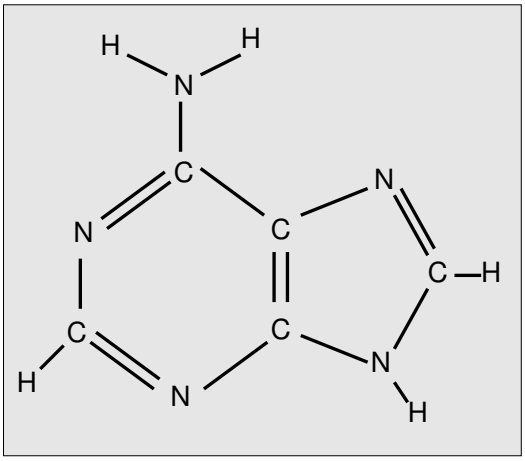

FIG. 31: Molecular structure of the purine base adenine (6-aminopurine, C_5,H_5N_5).

specified, the relative positions of the adenine molecules could not be determined. Still, the symmetry constraints on the adsorbate positions suggested that the adenine layer assembled in the form of centrosymmetrical hydrogen-bonded dimers.

It is true that it is possible to calculate the energetically most favorable structure by classical force field techniques [199, 200], however, these calculations do not yield any information about the electronic structure of the adsorbed molecules. They are useful in order to estimate the stability of possible adsorbate structures, but it is not really possible to assess whether their results are in agreement with STM experiments that do not have any atomic resolution. Thus, the force field techniques can not be used as a tool to analyse and interprete the STM images. However, for a complete understanding of the organic layers the effect of directed molecular bonds on the self-assembly and the STM-imaging process should be clarified. There is an additional problem in the STM imaging process, namely that the contrast in the STM images can depend on the scanning direction in the experiments [193]. This effect has not been appropriately investigated by first-principles calculations so far.

With DFT methods, it has become possible to address self-assemblied organic overlayers on surfaces [196, 201]. In particular, the DFT calculations also yield information on the electronic structure of the systems which makes it possible to simulate STM images. Within the Tersoff-Hamann picture [6], the tunneling current is simply proportional to the local density of states *of the surface* close to the Fermi energy at the position of the tip. There are more sophisticated DFT-based approaches to simulate STM images that also take into account the orbitals of the surface and the STM tip [202], but usually the simple Tersoff-Hamann picture is surprisingly successful and accurate.

A simulated STM image based on DFT calculations is shown in Fig. 32. The configuration space of possible

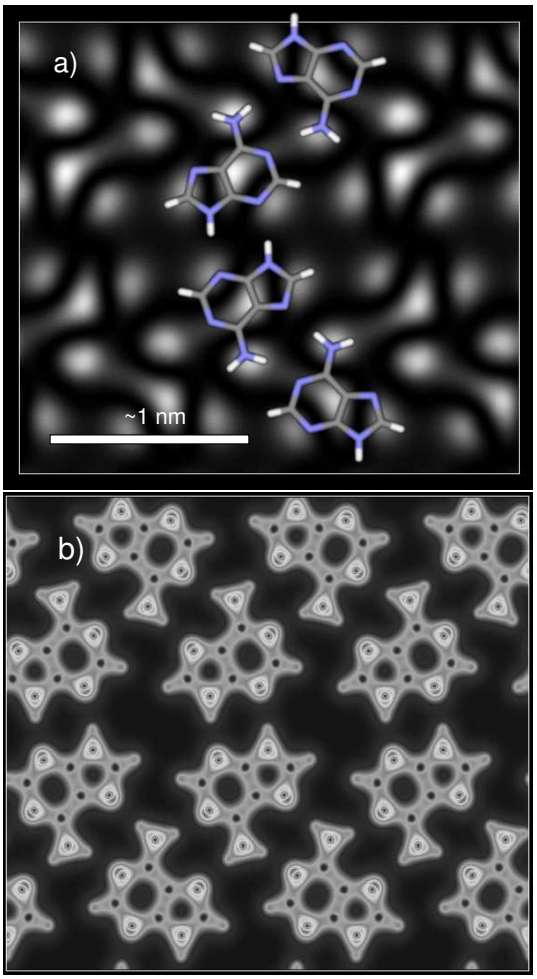

FIG. 32: Calculated structure of adsorbed adenine. a) simulated STM image according to the Tersoff-Hamann picture, i.e. the LDOS of the HOMO band is plotted. In addition, the structure of adsorbed adenine molecules is indicated; b) total charge density (courtesy of T. Markert).

adsorbate arrangements is immense. Therefore the DFT structure optimization has been done using the results of force-field calculations as an initial guess. It turned out that the optimized structures of the DFT and the force-field calculations are rather similar. However, it should be emphasized again that the force-field calculations do not yield any information on the electronic structure. What is plotted in Fig. 32a is the local density of states of the HOMO band at some distance from the surface. In addition, the molecular structure of the adenine molecules is shown indicating the hydrogen-bonded dimer structure. It is obvious that from the STM simulation alone the molecular structure could not have been deduced because there is no one-to-one correspondence between regions of high local density of states and the atomic arrangement. In Fig. 32b, the total charge density is plotted. The comparison between both panels shows that the regions of high local density of states of the HOMO band do also not necessarily coincide with maxima in the *total* charge density. This again confirms that indeed the realistic simulation of STM images is needed in order to deduce the atomistic structure of organic layers from STM experiments.

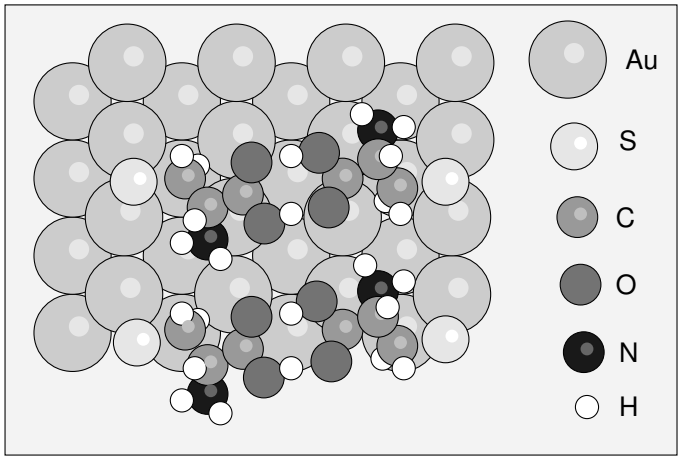

FIG. 33: The energetically most stable configuration of the amino acid cysteine on Au(110) calculated by DFT calculations [195]. It corresponds to two units of the double row structure of D cysteine.

The adsorption of cysteine ($HS\text{-}CH_2\text{-}CH(NH_2)\text{-}COOH$), an naturally occuring amino acid that has been briefly mentioned in the previous section, on the missing-row reconstructed Au(110) surface has been investigated by both STM experimentes and DFT calculations [122, 195]. Cysteine exists in two different so-called enantiomeric forms, L-cysteine and D-cysteine, i.e. two forms that are each others' mirror image with different chirality. In the STM experiments, both extended unidirectional molecular double rows as well as isolated dimers have been found. As far as the dimers are concerned, the DFT calculations have found that they are stabilized by forming double hydrogen bonds between their carboxylic group, as can be seen in Fig. 33. The STM experiments have found a high stereoselectivity in the dimerization of adsorbed cysteine molecules on the Au(110) surface, i.e. only either LL pairs or DD pairs have been identified.

According to DFT calculations, cysteine, like other thiols [203], binds rather strongly via the formation of S-Au bonds. As far as the dimers are concerned, their structure is also stabilized by amino–gold and carboxylic–carboxylic bonds. The presence of sulfur causes the formation of four vacancies on the gold rows of the (110) surface upon the adsorption of the dimers because of the tendency of sulfur to bind to low-coordinated atoms. Now in any possible LD dimer adsorption structure, at least one of these bonds is lost which makes the LD dimer energetically unfavourable. This explains why only LL or DD pairs have been observed in the STM experiments.

As for the double rows of cysteine on Au(110), their energetically most stable structure is shown in Fig. 33. In fact, the adsorption of cysteine leads to the lifting of the (2×1) missing-row reconstruction of the Au(110) surface.

However, there are no strong covalent or hydrogen bonds between the repeat units of the double rows. Also the dipole-dipole interactions between two adjacent units are fairly small.

Instead, it is the molecule induced surface rearrangement that is the driving force for the formation of the extended molecular rows [195]. The formation of a four-adatom vacancy on Au(110) in order to nucleate the first repeat unit of the double row is energetically rather costly, 0.9 eV. However, the energetic cost is only 0.4 eV for expanding a double row already formed. This is so because the formation of a Au vacancy adjacent to an existing vacancy requires much less energy than the formation of an isolated vacancy. Hence ones a first double-row unit has been formed, it is energetically favorable for additional cysteine dimers to attach to the existing dimer instead of forming isolated adsorbates. Thus unidirectional, self-assemblied molecular nanowires can be formed even in the absence of any significant direct adsorbate-adsorbate interaction along the growth direction.

VI. CONCLUSIONS AND OUTLOOK

In this chapter, theoretical studies of the adsorption of atoms and molecules at nanostructured surfaces using first-principles electronic structure methods have been reviewed. Such studies have only become possible in the last ten years because of their high computational demand. Although the size of the nanostructures treated in these studies is still limited [149, 164, 170], important qualitative concepts can be derived from these calculations. This is mainly due to the microscopic resolution of the calculations as far as both the geometric as well as the electronic structure of the studied systems is concerned.

Nanostructured surface often exhibit an enhanced interaction with adsorbates and a higher activity for certain reactions. An important aspect for the explanation of this high reactivity is the large number of low-coordinated atoms in nanostructures [146]. Many theoretical studies have shown that their is indeed a correlation between the low coordination of substrate atoms and a strong interaction with adsorbates. However, low coordination alone is often not sufficient for a strong interaction [147]. There are counter-examples of low-coordinated sites at nanostructured surfaces that do not bind adsorbates particularly well. Low-coordinated sites can lead to an enhanced electron density, but it is obviously also the nature of the orbitals localized at the low-coordinated sites that is important for the bonding of adsorbates.

In the future, first-principles electronic structure calculations will be able to address larger and larger systems due to the ongoing improvement in the computer power and the development of more efficient algorithms. This will certainly lead to further progress, as far as the microscopic analysis and understanding of nanostructures on surfaces and their reactivity is concerned. As already mentioned, the description of nanostructured surfaces by *ab initio* electronic structure calculations is a relatively new field. The first applications reviewed in this contribution have concentrated on a small number of particularly interesting systems such as Au cluster supported by oxide surfaces because of their strongly modified properties compared to bulk substrates. Still, systematic studies, for example of the role of the support on the reactivity of metallic clusters, are missing. Furthermore, a fundamental understanding of the size dependence of the adsorption properties and the reactivity of supported clusters is lacking [1].

A subject that has not at all been addressed so far in theoretical studies is the dynamics and kinetics of the adsorption at nanostructured surfaces based on *ab initio*-derived interaction potentials [204, 205]. Due to the complexity of the nanostructures, this certainly requires an high-computational effort, but there are important issues which need to be resolved. Nanostructures often offer the energetically most favorable sites for adsorption. However, the adsorbates have to get to these sites before they can bind. Does this occur via diffusion, or are the adsorbates directly steered [206] towards these sites? Furthermore, atomic and molecular adsorption require the dissipation of the energy gained upon binding to the substrate [207]. The question is still open whether nanostructures on surfaces represent an efficient sink for energy transfer.

There are also important kinetic aspects of the adsorption and reaction of molecules on nanoparticles to be studied. For example, it has been suggested that the activity of a catalyst particle can be significantly enhanced because of kinetic effects related to the interplay of different facets [208] but it is not clear yet how general this mechanism is. Kinetic rates can be estimated from electronic structure calculations using efficient transition state search routines [209, 210] in combination with transition state theory [211]. Although computational demanding, only kinetic simulations would allow a true comparison between theory and experiments in which reaction rates are measured.

It will probably take some time before supported clusters with thousands of atoms can be handled by *ab initio* total-energy calculations. In order to be able to address larger system with first-principles electronic structure calculations, one can either wait for faster computers or try to improve the algorithms. One example of a very successful improvement is the already mentioned development of ultrasoft pseudopotentials [41] which made it possible to use much smaller plane-wave basis sets in the supercell calculations.

Another possibility to make the calculations faster is to run them in a massively parallel fashion on many processors. The computational bottleneck in massively parallel implementations is usually the communication, i.e. the exchange of data between different processor. This

problem could in principle be avoided by so-called O(N) (order N) methods [212]. These methods take advantage of the localization properties of the fundamental interactions in materials [213]. Thus they are able to exhibit linear scaling with respect to the size of the system, i.e. their computational effort rises linearly with the number N of considered electrons or atoms in the calculations.

Due to the locality of the algorithm only little communication is needed between the processors that treat each some localized region of the system. This makes O(N) methods very suitable for massively parallel implementations. However, O(N) applications so far have been mainly based on tight-binding [214] or semiempirical descriptions. This is due to the fact that there are still problems as far as the implementation of linear-scaling methods in DFT codes is concerned [212].

However, it is questionable whether large-scale *ab initio* total-energy calculations are really neccessary for a deeper understanding of nanostructured surfaces. The more complex a system is, the harder it is to analyse its basic properties and to derive general principles. The important role of special sites and configurations of nanostructures, e.g., can already be investigated using smaller systems, as illustrated in this review, and other aspects of the nanostructures might be treated by more efficient, approximate methods such as multi-scale methods.

In the multi-scale approach, different aspects of a certain system are treated within different levels of microscopic accuracy [10, 215]. For example, in the theoretical description of large biomolecular systems so-called QM/MM (Quantum Mechanics/Molecular Mechanics) hybrid methods [216] have been successfully used for, e.g., the simulation of enzymatic systems [217]. These methods are based on a mixed quantum-classical embedding scheme in which the active center treated by first-principles electronic structure methods is embedded in a classical potential of the remaining atoms at the periphery.

Progress is also needed as far as the exchange-correlation functionals used in DFT calculations are concerned. GGA-DFT calculations are still not reliable for certain systems [45]. There are attempts to improve the accuracy of the functionals, for example by constructing so-called meta-GGA's [37]. However, they require a second order gradient expansion which makes them computationally less efficient. Consequently, they have not found a wide-spread recognition. Another approach is to include the so-called exact exchange in the DFT calculations by evaluating the corresponding exchange integral [218, 219]. This is again computationally rather demanding, and some progress in the efficient implementation is needed before this ansatz will experience a widespread use.

Another problem of current exchange-correlation functionals is that the van der Waals and hydrogen bond interaction are not properly described. This is closely related to the fact that in the LDA and the GGA the exchange-correlation hole is still localized. Therefore the effective electron potential outside of a metal falls off exponentially and not proportional to $1/z$. Although the van der Waals interaction is relatively weak, it is of relevance in the adsorption of large organic molecules which do not form any covalent bonds with the substrate. Thus a proper description of the van der Waals interaction is of importance for the *ab initio* description of the nanostructuring of surfaces by organic templates. There have been attempts to include the van der Waals interaction in density functional theory [220, 221]. However, these approaches require the introduction of an explicit van der Waals density functional. This leads to an increased computational effort which has prevented its implementation in standard DFT codes.

In spite of the technical obstacles, there will certainly be a growing number of first-principles studies addressing the adsorption on nanostructured surfaces since the interest in nanostructured surfaces and their technological applications will still increase. Although there is also significant progress in the experimental techniques, theoretical studies will remain to be an indispensable tool for the interpretation and analysis of structures and processes on the nano-scale. We will even see closer and closer collaborations between theory and experiment in the future. The theoretical investigation of adsorption on nanostructured surfaces is certainly a challenging and demanding research field, but at the same time it is an exciting and rewarding area that will prosper in the years to come.

Acknowledgments

It is a pleasure to acknowledge all the co-workers and friends whom I have worked with and who have contributed to my work. For the particular subject covered in this chapter I have greatly benefited from the insights shared with me by Wilhelm Brenig, Andreas Eichler, Jürgen Hafner, Peter Jakob, Bjørk Hammer, Wolfgang Heckl, Ulrich Höfer, Peter Kratzer, Georg Kresse, Eckhard Pehlke, Matthias Scheffler, and Ulrich Stimming. I also want to thank my coworkers in my research group at the Technical University of Munich who carried out research projects in the field of adsorption at nanostructured surfaces, Markus Lischka, Christian Mosch and Ata Roudgar. They all did a great job.

A significant fraction of this review has been written during my stay in the group of Prof. Horia Metiu at the Chemistry Department of the University of California at Santa Barbara. I thank him for his hospitality and for many fruitful discussions.

[1] C. R. Henry, Surf. Sci. Rep. **31**, 235 (1998).
[2] K. H. Hansen, S. Stempel, E. Lægsgaard, M. Bäumer, and H.-J. Freund, Phys. Rev. Lett. **83**, 4120 (1999).
[3] H.-J. Freund, Surf. Sci. **500**, 271 (2002).
[4] A. T. Bell, Science **299**, 1688 (2003).
[5] G. Binnig, H. Rohrer, C. Gerber, and E. Weibel, Phys. Rev. Lett. **49**, 57 (1982).
[6] J. Tersoff and D. R. Hamann, Phys. Rev. Lett. **50**, 1998 (1983).
[7] Y. L. Wang, H. J. Gao, H. M. Guo, H. W. Liu, I. G. Batyrev, W. E. McMahon, and S. B. Zhang, Phys. Rev. B **70**, 073312 (2004).
[8] A. Sanchez, S. Abbet, U. Heiz, W.-D. Schneider, H. Häkkinen, R. N. Barnett, and U. Landman, J. Phys. Chem. A **103**, 9573 (1999).
[9] A. Groß, Surf. Sci. **500**, 347 (2002).
[10] C. Stampfl, M. V. Ganduglia-Pirovano, K. Reuter, and M. Scheffler, Surf. Sci. **500**, 368 (2002).
[11] A. Szabo and N. S. Ostlund, *Modern quantum chemistry: introduction to advanced electronic structure theory*, McGraw-Hill, New York, 1989.
[12] P. Hohenberg and W. Kohn, Phys. Rev. **136**, B864 (1964).
[13] W. Kohn and L. Sham, Phys. Rev. **140**, A1133 (1965).
[14] W. Kohn, Rev. Mod. Phys. **71**, 1253 (1999).
[15] R. M. Dreizler and E. K. U. Gross, *Density Functional Theory: An Approach to the Quantum Many-Body Problem*, Springer, 1990.
[16] A. Groß, *Theoretical surface science – A microscopic perspective*, Springer, Berlin, 2002.
[17] P. Gambardella, Ž. Šljivančanin, B. Hammer, M. Blanc, K. Kuhnke, and K. Kern, Phys. Rev. Lett. **87**, 056103 (2001).
[18] M. Valden, X. Lai, and D. W. Goodman, Science **281**, 1647 (1998).
[19] B. Hammer, K. Jacobsen, and J. Nørskov, Phys. Rev. Lett. **69**, 1971 (1992).
[20] B. Hammer, M. Scheffler, K. Jacobsen, and J. Nørskov, Phys. Rev. Lett. **73**, 1400 (1994).
[21] J. A. White, D. M. Bird, M. C. Payne, and I. Stich, Phys. Rev. Lett. **73**, 1404 (1994).
[22] S. Wilke and M. Scheffler, Surf. Sci. **329**, L605 (1995).
[23] P. J. Feibelman, S. Esch, and T. Michely, Phys. Rev. Lett. **77**, 2257 (1996).
[24] M. Haruta, Catal. Today **36**, 153 (1997).
[25] M. Haruta, CatTech **6**, 102 (2002).
[26] K. Raghavachari and J. Anderson, J. Phys. Chem. **100**, 12960 (1996).
[27] J. A. Pople, Rev. Mod. Phys. **71**, 1267 (1999).
[28] G. W. Trucks, K. Raghavachari, G. S. Higashi, and Y. J. Chabal, Phys. Rev. Lett. **65**, 504 (1990).
[29] J. L. Whitten and H. Yang, Surf. Sci. Rep. **24**, 55 (1996).
[30] B. Hammer, L. B. Hansen, and J. K. Nørskov, Phys. Rev. B **59**, 7413 (1999).
[31] P. J. Feibelman, B. Hammer, J. K. Nørskov, F. Wagner, M. Scheffler, R. Stumpf, R. Watwe, and J. Dumesic, J. Phys. Chem. B **105**, 4018 (2001).
[32] E. H. Lieb, Rev. Mod. Phys. **53**, 603 (1981).
[33] J. P. Perdew, J. A. Chevary, S. H. Vosko, K. A. Jackson, M. R. Pederson, D. J. Singh, and C. Fiolhais, Phys. Rev. B **46**, 6671 (1992).
[34] A. D. Becke, Phys. Rev. A **38**, 3098 (1988).
[35] C. Lee, W. Yang, and R. Parr, Phys. Rev. B **37**, 785 (1988).
[36] J. P. Perdew, K. Burke, and M. Ernzerhof, Phys. Rev. Lett. **77**, 3865 (1996).
[37] J. P. Perdew, S. Kurth, A. Zupan, and P. Blaha, Phys. Rev. Lett. **82**, 2544 (1999).
[38] J. Tao, J. P. Perdew, V. N. Staroverov, and G. E. Scuseria, Phys. Rev. Lett. **91**, 146401 (2003).
[39] M. Fuchs and M. Scheffler, Comput. Phys. Commun. **119**, 67 (1999).
[40] P. E. Blöchl, Phys. Rev. B **50**, 17953 (1994).
[41] D. Vanderbilt, Phys. Rev. B **41**, 7892 (1990).
[42] G. Kresse and D. Joubert, Phys. Rev. B **59**, 1758 (1999).
[43] G. Kresse and J. Furthmüller, Phys. Rev. B **54**, 11169 (1996).
[44] M. Bockstedte, A. Kley, J. Neugebauer, and M. Scheffler, Comput. Phys. Commun. **107**, 187 (1997).
[45] B. Hammer, L. B. Hansen, and J. K. Nørskov, Phys. Rev. B **59**, 7413 (1999).
[46] A. Bogicevic, S. Ovesson, P. Hyldgaard, B. I. Lundqvist, H. Brune, and D. R. Jennison, Phys. Rev. Lett. **85**, 1910 (2000).
[47] B. Hammer and J. K. Nørskov, Surf. Sci. **343**, 211 (1995).
[48] B. Hammer and J. K. Nørskov, Nature **376**, 238 (1995).
[49] K. Fukui, Science **218**, 747 (1982).
[50] R. Hoffmann, Rev. Mod. Phys. **60**, 601 (1988).
[51] B. Hammer, O. H. Nielsen, and J. K. Nørskov, Catal. Lett. **46**, 31 (1997).
[52] V. Pallassana, M. Neurock, L. B. Hansen, B. Hammer, and J. K. Nørskov, Phys. Rev. B **60**, 6146 (1999).
[53] M. Mavrikakis, B. Hammer, and J. K. Nørskov, Phys. Rev. Lett. **81**, 2819 (1998).
[54] A. Roudgar and A. Groß, Phys. Rev. B **67**, 033409 (2003).
[55] A. Roudgar and A. Groß, J. Electronal. Chem. **548**, 121 (2003).
[56] M. Lischka and A. Groß, Phys. Rev. B **65**, 075420 (2002).
[57] N. W. Ashcroft and N. D. Mermin, *Solid State Physics*, Saunders College, Philadelphia, 1976.
[58] B. Lang, R. W. Joyner, and G. A. Somorjai, Surf. Sci **30**, 440 (1972).
[59] R. Q. Hwang, J. Schröder, C. Günther, and R. J. Behm, Phys. Rev. Lett. **67**, 3279 (1991).
[60] V. I. Anisimov, F. Aryasetiawan, and A. I. Lichtenstein, J. Phys.: Condens. Matter **9**, 767 (1997).
[61] G. Kresse, A. Gil, and P. Sautet, Phys. Rev. B **68**, 073401 (2003).
[62] A. C. Luntz, M. D. Williams, and D. S. Bethune, J. Chem. Phys. **89**, 4381 (1988).
[63] W. Wurth, J. Stöhr, P. Feulner, X. Pan, K. R. Bauchspiess, Y. Baba, E. Hudel, G. Rocker, and D. Menzel, Phys. Rev. Lett. **65**, 2426 (1990).
[64] C. T. Rettner and C. B. Mullins, J. Chem. Phys. **94**, 1626 (1991).
[65] J. Wintterlin, R. Schuster, and G. Ertl, Phys. Rev. Lett. **77**, 123 (1996).

[66] B. C. Stipe, M. A. Rezaei, W. Ho, S. Gao, M. Persson, and B. I. Lundqvist, Phys. Rev. Lett. **78**, 4410 (1997).

[67] P. D. Nolan, B. R. Lutz, P. L. Tanaka, J. E. Davis, and C. B. Mullins, J. Chem. Phys. **111**, 3696 (1999).

[68] A. Eichler and J. Hafner, Phys. Rev. Lett. **79**, 4481 (1997).

[69] A. Eichler, F. Mittendorfer, and J. Hafner, Phys. Rev. B **62**, 4744 (2000).

[70] A. Groß, A. Eichler, J. Hafner, M. J. Mehl, and D. A. Papaconstantopoulos, Surf. Sci. **539**, L542 (2003).

[71] Ž. Šljivančanin and B. Hammer, Surf. Sci. **515**, 235 (2002).

[72] S. Dahl, A. Logadottir, R. C. Egeberg, J. H. Larsen, I. Chorkendorff, E. Törnqvist, and J. K. Nørskov, Phys. Rev. Lett. **83**, 1814 (1999).

[73] S. Dahl, E. Törnqvist, and I. Chorkendorff, J. Catal. **192**, 381 (2000).

[74] K. Jacobi, H. Dietrich, and G. Ertl, Appl. Surf. Sci. **121/122**, 558 (1997).

[75] S. Dahl, P. A. Taylor, E. Törnqvist, and I. Chorkendorff, J. Catal. **178**, 679 (1998).

[76] A. Logadottir and J. K. Nørskov, J. Catal. **220**, 273 (2003).

[77] J. J. Mortensen, B. Hammer, and J. Nørskov, Phys. Rev. Lett. **80**, 4333 (1998).

[78] B. Hammer, Phys. Rev. Lett **83**, 3681 (1999).

[79] T. Zambelli, J. Wintterlin, J. Trost, and G. Ertl, Science **273**, 1688 (1996).

[80] K. Christmann, Surf. Sci. Rep. **9**, 1 (1988).

[81] A.-S. Mårtensson, C. Nyberg, and S. Andersson, Phys. Rev. Lett. **57**, 2045 (1986).

[82] K. Svensson, L. Bengtsson, J. Bellman, M. Hassel, M. Persson, and S. Andersson, Phys. Rev. Lett. **83**, 124 (1999).

[83] L. Bengtsson, K. Svensson, M. Hassel, J. Bellman, M. Persson, and S. Andersson, Phys. Rev. B **61**, 16921 (2000).

[84] P. K. Schmidt, K. Christmann, G. Kresse, J. Hafner, M. Lischka, and A. Groß, Phys. Rev. Lett. **87**, 096103 (2001).

[85] S. Wilke and M. Scheffler, Phys. Rev. B **53**, 4926 (1996).

[86] W. Dong, V. Ledentu, P. Sautet, A. Eichler, and J. Hafner, Surf. Sci. **411**, 123 (1998).

[87] A. Groß, Appl. Phys. A **67**, 627 (1998).

[88] X.-G. Zhang et al., Phys. Rev. Lett. **67**, 1298 (1991).

[89] M. Lischka, C. Mosch, and A. Groß, Surf. Sci. **570**, 227 (2004).

[90] W. Dong and J. Hafner, Phys. Rev. B **56**, 15396 (1997).

[91] V. Ledentu, W. Dong, and P. Sautet, Surf. Sci. **412**, 518 (1998).

[92] A. Dedieu, Chem. Rev. **100**, 543 (2000).

[93] M. Lischka and A. Groß, Hydrogen on palladium: a model system for the interaction of atoms and molecules with metal surfaces, in *Recent Developments in Vacuum Science and Technology*, edited by J. Dabrowski, pages 111–132, Research Signpost, Kerala (India), 2003.

[94] R. F. Service, Science **305**, 958 (2004).

[95] R. J. Behm, K. Christmann, G. Ertl, and M. A. Van Hove, J. Chem. Phys. **73**, 2984 (1980).

[96] A. Eichler and J. Hafner, Phys. Rev. B **57**, 10110 (1998).

[97] P. Hu, D. A. King, M.-H. Lee, and M. C. Payne, Chem. Phys. Lett. **246**, 73 (1995).

[98] M. Kittel, R. Terborg, M. Polcik, A. M. Bradshaw, R. L. Toomes, D. P. Woodruff, and E. Rotenberg, Surf. Sci. **511**, 34 (2002).

[99] H. S. Kato, H. Okuyama, J. Yoshinubo, and M. Kawai, Surf. Sci. **513**, 239 (2002).

[100] T. E. Madey, J. T. Yates, Jr., A. M. Bradshaw, and F. M. Hoffmann, Surf. Sci. **89**, 370 (1979).

[101] H. Conrad, G. Ertl, J. Koch, and E. E. Latta, Surf. Sci. **43**, 462 (1974).

[102] P. K. Schmidt, *Wechselwirkung von Wasserstoff mit einer Pd(210)- und Ni(210)-Oberfläche*, PhD thesis, Freie Universität Berlin, 2002.

[103] E. Christoffersen, P. Stoltze, and J. K. Nørskov, Surf. Sci. **505**, 200 (2002).

[104] B. Hammer, J. Catal. **199**, 171 (2001).

[105] E. Christoffersen, P. Liu, A. Ruban, H. L. Skriver, and J. K. Nørskov, J. Catal. **199**, 123 (2001).

[106] C. M. Wei, A. Groß, and M. Scheffler, Phys. Rev. B **57**, 15572 (1998).

[107] L. Savio, L. Vattuone, and M. Rocca, Phys. Rev. Lett. **87**, 276101 (2001).

[108] L. Savio, L. Vattuone, and M. Rocca, J. Phys.: Condens. Matter **14**, 6065 (2002).

[109] L. Vattuone, L. Savio, and M. Rocca, Phys. Rev. Lett. **90**, 228302 (2003).

[110] N. Bonini, A. Kokalj, A. Dal Corso, S. de Gironcoli, and S. Baroni, Phys. Rev. B **69**, 195401 (2004).

[111] A. Kokalj, N. Bonini, A. Dal Corso, S. de Gironcoli, and S. Baroni, Surf. Sci. **566**, 1107 (2004).

[112] T. Schimizu and M. Tsukada, Surf. Sci. **295**, L1017 (1993).

[113] L. Delle Site and D. Sebastiani, Phys. Rev. B **70**, 115401 (2004).

[114] J. M. Thomas and W. J. Thomas, *Principles and Practice of Heterogeneous Catalysis*, VCH-Wiley, Weinheim, 1997.

[115] A. Kokalj, A. Dal Corso, S. de Gironcoli, and S. Baroni, J. Phys. Chem. B **106**, 9839 (2002).

[116] A. Kokalj, A. Dal Corso, S. de Gironcoli, and S. Baroni, Surf. Sci. **566**, 1018 (2004).

[117] Ž. Šljivančanin, K. V. Gothelf, and B. Hammer, J. Am. Chem. Soc. **124**, 14789 (2002).

[118] C. F. McFadden, P. S. Cremer, and A. J. Gellman, Langmuir **12**, 2483 (1996).

[119] G. A. Attard, J. Phys. Chem. B **105**, 3158 (2001).

[120] Ž. Šljivančanin and B. Hammer, Phys. Rev. B **65**, 085414 (2002).

[121] C. D. Bain, J. Evall, and G. M. Whitesides, J. Am. Chem. Soc. **111**, 7155 (1989).

[122] A. Kühnle, T. R. Linderoth, B. Hammer, and F. Besenbacher, Nature **415**, 891 (2002).

[123] T. D. Booth, D. Wahnon, and I. Wainer, Chirality **9**, 96 (1997).

[124] G. S. Higashi, Y. J. Chabal, G. W. Trucks, and K. Raghavachari, Appl. Phys. Lett. **56**, 656 (1990).

[125] E. Pehlke and M. Scheffler, Phys. Rev. Lett. **74**, 952 (1995).

[126] A. Groß, M. Bockstedte, and M. Scheffler, Phys. Rev. Lett. **79**, 701 (1997).

[127] C. Filippi, S. B. Healy, P. Kratzer, E. Pehlke, and M. Scheffler, Phys. Rev. Lett. **89**, 166102 (2002).

[128] P. Kratzer, E. Pehlke, M. Scheffler, M. B. Raschke, and U. Höfer, Phys. Rev. Lett. **81**, 5596 (1998).

[129] E. Pehlke and J. Tersoff, Phys. Rev. Lett. **67**, 1290

(1991).
[130] E. Pehlke and P. Kratzer, Phys. Rev. B **59**, 2790 (1999).
[131] P. Krüger and J. Pollmann, Phys. Rev. Lett. **74**, 1155 (1995).
[132] M. Rohlfing, P. Krüger, and J. Pollmann, Phys. Rev. B **52**, 1905 (1995).
[133] E. Pehlke, Phys. Rev. B **62**, 12932 (2000).
[134] A. Biedermann, E. Knoesel, Z. Hu, and T. F. Heinz, Phys. Rev. Lett. **83**, 1810 (1999).
[135] M. Dürr, Z. Hu, A. Biedermann, U. Höfer, and T. F. Heinz, Phys. Rev. Lett. **88**, 046104 (2002).
[136] W. Brenig and M. F. Hilf, J. Phys. Condens. Mat. **13**, R61 (2001).
[137] K. W. Kolasinski, W. Nessler, K.-H. Bornscheuer, and E. Hasselbrink, J. Chem. Phys. **101**, 7082 (1994).
[138] P. Bratu, K. L. Kompa, and U. Höfer, Chem. Phys. Lett. **251**, 1 (1996).
[139] K. W. Kolasinski, W. Nessler, A. de Meijere, and E. Hasselbrink, Phys. Rev. Lett. **72**, 1356 (1994).
[140] U. Landman and L. WD, Faraday Diss. **125**, 1 (2004).
[141] S. J. Tauster, S. C. Fung, and R. L. Garten, J. Am. Chem. Soc. **100**, 170 (1978).
[142] D. R. Jennison, O. Dulub, W. Hebenstreit, and U. Diebold, Surf. Sci. **106**, L677 (2001).
[143] P. Pyykko, Angew. Chemie, Int. Ed. **43**, 4412 (2004).
[144] G. Mills, M. S. Gordon, and H. Metiu, J. Chem. Phys. **118**, 4198 (2003).
[145] S. A. Varganov, R. M. Olson, M. S. Gordon, and H. Metiu, J. Chem. Phys. **119**, 2531 (2003).
[146] N. Lopez and J. K. Nørskov, J. Am. Chem. Soc. **124**, 11262 (2002).
[147] S. Chrétien, M. S. Gordon, and H. Metiu, J. Chem. Phys. **121**, 3756 (2004).
[148] B. Yoon, H. Häkkinen, and U. Landman, J. Phys. Chem. A **107**, 4066 (2003).
[149] G. Mills, M. S. Gordon, and H. Metiu, Chem. Phys. Lett. **359**, 493 (2002).
[150] Y. Zhang, A. Kolmakov, S. Chretien, H. Metiu, and M. Moskovits, Nano Lett. **4**, 403 (2004).
[151] M. Mavrikakis, P. Stoltz, and J. K. Nørskov, Catal. Lett. **64**, 101 (2000).
[152] N. Lopez, T. V. W. Janssens, B. S. Clausen, Y. Xu, M. Mavrikakis, T. Bligaard, and J. K. Nørskov, J. Catal. **223**, 232 (2004).
[153] L. Piccolo, D. Loffreda, F. J. C. S. Aires, C. Deranlot, Y. Jugnet, P. Sautet, and J. C. Bertolini, Surf. Sci. **566**, 995 (2004).
[154] Z.-P. Liu, P. Hu, and A. Alavi, J. Am. Chem. Soc. **124**, 11262 (2002).
[155] Y. Wang and G. S. Hwang, Surf. Sci. **542**, 72 (2003).
[156] A. Vittadini and A. Selloni, J. Chem. Phys. **117**, 353 (2002).
[157] N. Lopez, J. K. Nørskov, T. V. W. Janssens, A. Carlsson, A. Puig-Molina, B. S. Clausen, and J. D. Grunwaldt, J. Catal. **225**, 86 (2004).
[158] L. M. Molina and B. Hammer, Phys. Rev. Lett. **90**, 206102 (2003).
[159] L. M. Molina, M. D. Rasmussen, and B. Hammer, J. Chem. Phys. **120**, 7673 (2004).
[160] L. M. Molina and B. Hammer, Phys. Rev. B **69**, 155424 (2004).
[161] M. D. Rasmussen, L. M. Molina, and B. Hammer, J. Chem. Phys. **120**, 988 (2004).
[162] M. S. Chen and D. W. Goodman, Science **306**, 252 (2004).
[163] H. Häkkinen, S. Abbet, A. Sanchez, U. Heiz, and U. Landman, Angew. Chem. Int. Ed. **42**, 1297 (2003).
[164] S. Abbet, U. Heiz, A. M. Ferrari, L. Giordano, C. Di Valentin, and G. Pacchioni, Thin Solid Films **400**, 37 (2001).
[165] P. M. Ajayan and L. D. Marks, Nature **338**, 139 (1989).
[166] R. J. H. Grisel and B. E. Nieuwenhuys, J. Catal. **199**, 48 (2001).
[167] P. Broqvist, L. M. Molina, H. Grönbeck, and H. B., J. Catal. **227**, 217 (2004).
[168] L. Giordano, G. Pacchioni, F. Illas, and R. N., Surf. Sci. **499**, 73 (2002).
[169] L. Giordano, G. Pacchioni, A. M. Ferrari, F. Illas, and R. N., Surf. Sci. **473**, 213 (2001).
[170] A. Roudgar and A. Groß, Surf. Sci. **559**, L180 (2004).
[171] D. M. Kolb, Surf. Sci. **500**, 722 (2002).
[172] D. M. Kolb, R. Ullmann, and T. Will, Science **275**, 1097 (1997).
[173] G. E. Engelmann, J. C. Ziegler, and D. M. Kolb, J. Electrochem. Soc. **145**, L33 (1998).
[174] J. Meier, K. A. Friedrich, and U. Stimming, Faraday Discuss. **121**, 365 (2002).
[175] J. Meier, J. Schiotz, P. Liu, J. K. Nørskov, and U. Stimming, Chem. Phys. Lett. **390**, 440 (2004).
[176] D. M. Kolb, G. E. Engelmann, and J. C. Ziegler, Angew. Chemie, Int. Ed. **39**, 1123 (2000).
[177] M. G. Del Popolo, E. P. M. Leiva, H. Kleine, J. Meier, U. Stimming, M. Mariscal, and W. Schmickler, Appl. Phys. Lett. **81**, 2635 (2002).
[178] M. G. Del Popolo, E. P. M. Leiva, H. Kleine, J. Meier, U. Stimming, M. Mariscal, and W. Schmickler, Electrochim. Acta **48**, 1287 (2003).
[179] S. M. Foiles, M. I. Baskes, and M. S. Daw, Phys. Rev. B **33**, 7983 (1986).
[180] M. S. Daw, S. M. Foiles, and M. I. Baskes, Mater. Sci. Rep. **9**, 252 (1993).
[181] M. G. Del Popolo, E. P. M. Leiva, M. Mariscal, and W. Schmickler, Nanotechnology **14**, 1009 (2003).
[182] A. Roudgar, private communication.
[183] J. A. Rodriguez, Surf. Sci. Rep. **24**, 223 (1996).
[184] J. A. Rodriguez, J. Dvorak, T. Jirsak, and J. Hrbek, Surf. Sci. **315**, 315 (2001).
[185] Z. P. Chang, Z. Song, G. Liu, J. A. Rodriguez, and J. Hrbek, Surf. Sci. **512**, L353 (2002).
[186] S. Helveg, J. V. Lauritsen, E. Lægsgaard, I. Stensgaard, J. K. Nørskov, B. S. Clausen, H. Topsøe, and F. Besenbacher, Phys. Rev. Lett. **84**, 951 (2000).
[187] P. Liu, J. A. Rodriguez, J. T. Muckerman, and J. Hrbek, Surf. Sci. **530**, L313 (2003).
[188] P. Liu, J. A. Rodriguez, J. T. Muckerman, and J. Hrbek, Phys. Rev. B **67**, 155416 (2003).
[189] F. Rosei, M. Schunack, Y. Naitoh, P. Jiang, A. Gourdon, E. Lægsgaard, I. Stensgaard, C. Joachim, and F. Besenbacher, Prog. Surf. Sci. **71**, 95 (2003).
[190] S. J. Sowerby, W. M. Heckl, and G. B. Petersen, J. Mol. Evol. **43**, 419 (1996).
[191] W. M. Heckl, Molecular self-assembly and the origin of life, in *Astrobiology, The Quest for the Conditions of Life*, edited by G. Horneck and C. Baumstark-Khan, Springer, Berlin, 2002.
[192] S. J. Sowerby, M. Edelwirth, and W. M. Heckl, J. Phys. Chem. **102**, 5914 (1998).
[193] S. J. Sowerby, M. Edelwirth, M. Reiter, and W. M.

Heckl, Langmuir **14**, 5915 (1998).
[194] U. Ziener, J.-M. Lehn, A. Mourran, and M. Möller, Chem. Eur. J. **8**, 951 (2002).
[195] A. Kühnle, L. M. Molina, T. R. Linderoth, B. Hammer, and F. Besenbacher, Phys. Rev. Lett. **93**, 086101 (2004).
[196] S. Clair, S. Pons, A. P. Seitsonen, H. Brune, K. Kern, and J. V. Barth, J. Phys. Chem. B **108**, 14585 (2004).
[197] N. J. Tao and Z. Shi, J. Phys. Chem. **98**, 1464 (1994).
[198] J. Freund, M. Edelwirth, P. Kröbel, and W. M. Heckl, Phys. Rev. B **55**, 5394 (1997).
[199] M. Edelwirth, J. E. Freund, S. J. Sowerby, and W. M. Heckl, Surf. Sci. **417**, 201 (1998).
[200] K. Shinoda, W. Shinoda, C. C. Liew, S. Tsuzuki, Y. Morikawa, and M. Mikami, Surf. Sci. **556**, 109 (2004).
[201] T. H. Rod and J. K. Nørskov, Surf. Sci. **500**, 678 (2002).
[202] W. A. Hofer, A. S. Foster, and A. Shluger, Rev. Mod. Phys. **75**, 1287 (2003).
[203] L. M. Molina and B. Hammer, Chem. Phys. Lett. **360**, 264 (2002).
[204] A. Groß, Surf. Sci. Rep. **32**, 291 (1998).
[205] D. Marx and J. Hutter, Ab initio molecular dynamics: Theory and implementation, in *Modern Methods and Algorithms of Quantum Chemistry*, edited by J. Grotendorst, volume 3 of *NIC series*, pages 329–477, John von Neumann-Institute for Computing, Jülich, 2000.
[206] A. Groß, S. Wilke, and M. Scheffler, Phys. Rev. Lett. **75**, 2718 (1995).
[207] A. Groß, Dynamics of molecule-surface interactions from first principles, in *The Chemical Physics of Solid Surfaces*, edited by D. P. Woodruff, volume 11, chapter 1, Elsevier, Amsterdam, 2003.
[208] V. P. Zhdanov and B. Kasemo, Cat. Lett. **81**, 141 (2002).
[209] G. Henkelman and H. Jónsson, J. Chem. Phys. **111**, 7010 (1999).
[210] G. Henkelman, B. P. Uberuaga, and H. Jónsson, J. Chem. Phys. **113**, 9901 (2000).
[211] P. Hänngi, P. Talkner, and M. Borkovec, Rev. Mod. Phys. **62**, 251 (1990).
[212] S. Goedecker, Rev. Mod. Phys. **71**, 1085 (1999).
[213] W. Kohn, Phys. Rev. Lett. **76**, 3168 (1996).
[214] S. Goedecker and L. Colombo, Phys. Rev. Lett. **73**, 122 (1994).
[215] F. Starrost and E. A. Carter, Surf. Sci. **500**, 323 (2002).
[216] M. Eichinger, P. Tavan, J. Hutter, and M. Parrinello, J. Chem. Phys. **110**, 10452 (1999).
[217] P. Carloni and U. Röthlisberger, Simulations of enzymatic systems: Perspectives from car-parrinello molecular dynamics simulations, in *Theoretical Biochemistry – Processes and Properties of Biological Systems*, edited by L. Eriksson, page 215, Elsevier, Amsterdam, 2001.
[218] M. Stadele, J. A. Majewski, P. Vogl, and A. Görling, Phys. Rev. Lett. **79**, 2089 (1997).
[219] F. Della Sala and A. Görling, J. Chem. Phys. **118**, 10439 (2003).
[220] W. Kohn, Y. Meir, and D. Makarov, Phys. Rev. Lett. **80**, 4153 (1998).
[221] E. Hult, H. Rydberg, B. Lundqvist, and D. Langreth, Phys. Rev. B **59**, 4708 (1999).